Monthly Notices
of the
ROYAL ASTRONOMICAL SOCIETY

MNRAS **432,** 1845–1861 (2013) doi:10.1093/mnras/stt062
Advance Access publication 2013 May 11

The ATLAS^{3D} project – XIX. The hot gas content of early-type galaxies: fast versus slow rotators

Marc Sarzi,[1]⋆ Katherine Alatalo,[2] Leo Blitz,[2] Maxime Bois,[3] Frédéric Bournaud,[4] Martin Bureau,[5] Michele Cappellari,[5] Alison Crocker,[6] Roger L. Davies,[5] Timothy A. Davis,[7] P. T. de Zeeuw,[7,8] Pierre-Alain Duc,[4] Eric Emsellem,[7,9] Sadegh Khochfar,[10] Davor Krajnović,[7] Harald Kuntschner,[11] Pierre-Yves Lablanche,[2,9] Richard M. McDermid,[12] Raffaella Morganti,[13,14] Thorsten Naab,[15] Tom Oosterloo,[13,14] Nicholas Scott,[16] Paolo Serra,[13] Lisa M. Young[17]† and Anne-Marie Weijmans[18]‡

[1]*Centre for Astrophysics Research, University of Hertfordshire, Hatfield, Herts AL1 9AB, UK*
[2]*Department of Astronomy, Campbell Hall, University of California, Berkeley, CA 94720, USA*
[3]*Observatoire de Paris, LERMA and CNRS, 61 Av. de l'Observatoire, F-75014 Paris, France*
[4]*Laboratoire AIM Paris-Saclay, CEA/IRFU/SAp – CNRS – Université Paris Diderot, F-91191 Gif-sur-Yvette Cedex, France*
[5]*Sub-Department of Astrophysics, Department of Physics, University of Oxford, Denys Wilkinson Building, Keble Road, Oxford OX1 3RH, UK*
[6]*Department of Astronomy, University of Massachussets, Amherst, MA 01003, USA*
[7]*European Southern Observatory, Karl-Schwarzschild-Str. 2, D-85748 Garching, Germany*
[8]*Sterrewacht Leiden, Leiden University, Postbus 9513, NL-2300 RA Leiden, the Netherlands*
[9]*Université Lyon 1, Observatoire de Lyon, Centre de Recherche Astrophysique de Lyon and Ecole Normale Supérieure de Lyon, 9 avenue Charles André, F-69230 Saint-Genis Laval, France*
[10]*Max-Planck Institut für extraterrestrische Physik, PO Box 1312, D-85478 Garching, Germany*
[11]*Space Telescope European Coordinating Facility, European Southern Observatory, Karl-Schwarzschild-Str. 2, 85748 Garching, Germany*
[12]*Gemini Observatory, Northern Operations Centre, 670 N. A'ohoku Place, Hilo, HI 96720, USA*
[13]*Netherlands Institute for Radio Astronomy (ASTRON), Postbus 2, NL-7990 AA Dwingeloo, the Netherlands*
[14]*Kapteyn Astronomical Institute, University of Groningen, Postbus 800, NL-9700 AV Groningen, the Netherlands*
[15]*Max-Planck-Institut für Astrophysik, Karl-Schwarzschild-Str. 1, D-85741 Garching, Germany*
[16]*Centre for Astrophysics and Supercomputing, Swinburne University of Technology, PO Box 218, Hawthorn, VIC 3122, Australia*
[17]*Physics Department, New Mexico Institute of Mining and Technology, Socorro, NM 87801, USA*
[18]*Dunlap Institute for Astronomy and Astrophysics, University of Toronto, 50 St. George Street, Toronto, ON M5S 3H4, Canada*

Accepted 2013 January 8. Received 2012 December 17; in original form 2012 May 24

ABSTRACT

For early-type galaxies, the ability to sustain a corona of hot, X-ray-emitting gas could have played a key role in quenching their star formation history. A halo of hot gas may act as an effective shield against the acquisition of cold gas and can quickly absorb stellar mass loss material. Yet, since the discovery by the *Einstein Observatory* of such X-ray haloes around early-type galaxies, the precise amount of hot gas around these galaxies still remains a matter of debate. By combining homogeneously derived photometric and spectroscopic measurements for the early-type galaxies observed as part of the ATLAS^{3D} integral field survey with measurements of their X-ray luminosity based on X-ray data of both low and high spatial resolution (for 47 and 19 objects, respectively) we conclude that the hot gas content of early-type galaxies can depend on their dynamical structure. Specifically, whereas slow rotators generally have X-ray haloes with luminosity $L_{\rm X,\,gas}$ and temperature T values that are well in line with what is expected if the hot gas emission is sustained by the thermalization of the kinetic energy carried by the stellar mass loss material, fast rotators tend to display $L_{\rm X,\,gas}$

⋆ E-mail: m.sarzi@herts.ac.uk
† Adjunct astronomer with NRAO.
‡ Dunlap fellow.

values that fall consistently below the prediction of this model, with similar T values that do not scale with the stellar kinetic energy (traced by the stellar velocity dispersion) as observed in the case of slow rotators. Such a discrepancy between the hot gas content of slow and fast rotators would appear to reduce, or even disappear, for large values of the dynamical mass (above $\sim 3 \times 10^{11}$ $M_{\odot}$), with younger fast rotators displaying also somewhat larger $L_{X,\,gas}$ values possibly owing to the additional energy input from recent supernovae explosions. Considering that fast rotators are likely to be intrinsically flatter than slow rotators, and that the few $L_{X,\,gas}$-deficient slow rotators also happen to be relatively flat, the observed $L_{X,\,gas}$ deficiency in these objects would support the hypothesis whereby flatter galaxies have a harder time in retaining their hot gas, although we suggest that the degree of rotational support could further hamper the efficiency with which the kinetic energy of the stellar mass loss material is thermalized in the hot gas. We discuss the implications that a different hot gas content could have on the fate of both acquired and internally produced gaseous material, considering in particular how the $L_{X,\,gas}$ deficiency of fast rotators would make them more capable to recycle the stellar mass loss material into new stars than slow rotators. This would be consistent with the finding that molecular gas and young stellar populations are detected only in fast rotators across the entire ATLAS^{3D} sample, and that fast rotators tend to have a larger specific dust mass content than slow rotators.

Key words: galaxies: elliptical and lenticular, cD – galaxies: evolution – galaxies: formation – galaxies: ISM – X-rays: binaries – X-rays: galaxies.

1 INTRODUCTION

Early-type galaxies used to be regarded as purely stellar systems over the largest part of the last century, even though the presence of little or no interstellar medium in these old stellar systems was soon recognized as a problem by Faber & Gallagher (1976). Indeed, such a lack of gas contrasts with the notion that stars lose a considerable fraction of their initial mass during their evolution. In this context, the finding by the *Einstein Observatory* that early-type galaxies are surrounded by massive haloes of hot ($\sim 10^6$–10^7 K) X-ray-emitting gas (e.g. Forman et al. 1979) both changed our view of early-type galaxies and provided a possible solution to the problem posed by Faber & Gallagher, if a mechanism to heat the stellar ejecta to X-ray temperatures could be found. Around the same time, the advent of new and homogeneous sets of optical data for large numbers of early-type galaxies prompted the finding of a correlation between the X-ray luminosity of such haloes L_X and the optical luminosity L_B of the galaxies they contain (e.g. Forman, Jones & Tucker 1985; Trinchieri & Fabbiano 1985), which when interpreted led to a relatively simple model linking the hot gas reservoirs to the stellar mass loss material of early-type galaxies (e.g. Canizares, Fabbiano & Trinchieri 1987). According to this scenario, still part of the current consensus, the gas ejected from evolved stars and planetary nebulae collides and shocks with other ejecta or a pre-existing ambient gas until it is heated to the kinetic temperature that corresponds to the stellar velocity dispersion of a galaxy. Supernovae (SNe) explosions (in particular of Type Ia; e.g. Mathews & Loewenstein 1986; Ciotti et al. 1991) contribute to further heat this gas, but may lead also to its escape. This would have generally been the case when galaxies were young and SNe explosions more frequent, whereas today SNe-driven global outflows should be more restricted to the less massive systems. On the other hand, bigger galaxies can hold better to their hot gas, and in amounts that scale with their optical luminosity given the stellar origin of such a material.

Yet, despite its tremendous success in explaining the broad trend of the L_B–L_X relation, this idea alone does not account for the wide range of X-ray luminosities, of about two orders of magnitude, that is observed in galaxies of similar optical luminosity. A number of physical phenomena have been observed to enter the scatter of the $L_B - L_X$ relation (starting from the isophotal shape of galaxies; Bender et al. 1989) and examined to account for it (see, for example, the reviews of Mathews & Brighenti 2003; Pellegrini 2012). Earlier explanations invoked different degrees of ram-pressure stripping, since galaxies in dense galactic environment were found to be X-ray faint (White & Sarazin 1991), or different stages of the hot gas evolution caused by the steady decrease over time of the energy provided by SNe or the thermalization of the stellar motions, which by eventually falling short of the power required to extract the gas from a galaxy drives galaxies from an X-ray faint wind and outflow phase to an X-ray bright inflow phase (and at different speed for galaxies with different structural parameters such as central density, effective radius or kind of radial profile; Ciotti et al. 1991). Subsequently, the finding by Eskridge, Fabbiano & Kim (1995a,b) that S0s and flat Es show lower X-ray luminosities than rounder elliptical galaxies of the same optical luminosity prompted further theoretical studies concerning the role of intrinsic flattening (which reduces the binding energy of the hot gas and makes it harder to retain it; Ciotti & Pellegrini 1996) or rotation (Brighenti & Mathews 1996; D'Ercole & Ciotti 1998). More recent studies considered also the impact of secondary gas accretion events (Pipino et al. 2005) and showed the importance of contamination from the radiation of the intracluster medium (ICM, which originates most likely from cosmological flows; Mathews & Brighenti 2003) in the L_X measurements obtained from relatively shallow surveys (Matsushita 2001).

The launch of the *Chandra* and *XMM* space telescopes, with their higher spatial resolution, spectral range and sensitivity, has now made it possible to isolate the X-ray emission of galactic haloes from the signal of unresolved low-mass X-ray binaries (LMXBs), active galactic nuclei (AGN) or the ICM that otherwise enters the coarser *Einstein* or *ROSAT* measurements of L_X. These measurements are very expensive in terms of telescope time, however, and as a result the number of objects with pure $L_{X,\,gas}$ values for hot gas haloes is still quite limited. This is particular true considering that good quality and homogeneous optical data, as well as robust

distance estimates, are also highly desirable in order to understand what drives the scatter in the X-ray properties of galaxies. On the other hand, since also photometric and spectroscopic optical measurements for nearby galaxies are witnessing a quantum leap both in quality and sky coverage, it may be possible to make progress in this domain while still using L_X measurements based on *ROSAT* or *Einstein* data, which cover a large number of objects. This was for instance the case of the study of Ellis & O'Sullivan (2006), who used the near-infrared measurements from the Two Micron All Sky Survey (2MASS; Skrutskie et al. 2006) to revisit the stellar to X-ray luminosity relation while still using nearly all of the 401 early-type galaxies in the catalogue of O'Sullivan, Forbes & Ponman (2001), still as of today the largest compilation of L_X measurements obtained with *ROSAT* and *Einstein*.

By drawing on new optical data from the complete ATLAS^{3D} survey (Cappellari et al. 2011a, hereafter Paper I), in this paper we will use both such approaches to reconsider the origin of the scatter in the X-ray luminosity of early-type galaxies, starting from *ROSAT* or *Einstein* data for the total X-ray luminosity of 47 galaxies from the ATLAS^{3D} survey to then analyse a second ATLAS^{3D} subsample of 19 objects with consistent *Chandra* measurements of the X-ray luminosity of their hot gas. In particular, we will revisit the possible role of galactic rotation and flattening in driving the hot gas content of galaxies, building on the first observational tests of Pellegrini, Held & Ciotti (1997) and in light of the emerging distinction among early-type galaxies between a dominant population of fast-rotating objects (with regular velocity fields; Krajnović et al. 2011, hereafter Paper II) and a less common class of slowly rotating galaxies (often hosting kinematically distinct cores; Emsellem et al. 2011, hereafter Paper III). Fast and slow rotators are indeed not only likely to have formed in different ways (Cappellari et al. 2007; Emsellem et al. 2007) but also to have distinct distributions for their intrinsic shapes, with fast rotators being nearly as flat as spiral galaxies and slow rotators being much rounder and possibly triaxial (Weijmans et al., in preparation, but see already Cappellari et al. 2011b, hereafter Paper VII).

This paper is organized as follows. In Section 2 we define our two samples and the optical parameters from the ATLAS^{3D} survey that will be needed for our investigation. We derive our results in Section 3, considering first in Section 3.1 an ATLAS^{3D} subsample with X-ray measurements based on *ROSAT* and *Einstein* data. We then expand our analysis in Section 3.2 to ATLAS^{3D} galaxies with *Chandra* data, and further check in Section 3.3 the results from both Sections 3.1 and 3.2 using an additional but less homogeneous set of *Chandra* X-ray measurements from the literature. We discuss our findings in Section 4, and wrap up our conclusions in Section 5.

2 X-RAY DATA AND SAMPLES PROPERTIES

The two sets of galaxies that will be used in this work simply consist (a) of all the objects in the ATLAS^{3D} sample in Paper I for which O'Sullivan et al. (2001) provides a *ROSAT* or *Einstein* measurement for their L_X (considering only detections), and (b) of all the ATLAS^{3D} sample galaxies for which Boroson, Kim & Fabbiano (2011) could use *Chandra* data to separate the L_X contribution from the otherwise unresolved population of LMXBs and from the hot, X-ray-emitting gas. These two ATLAS^{3D} subsamples include 47 and 19 galaxies, respectively, and since the main difference between them is the spatial resolution of the X-ray data from the literature that were used to compile them, hereafter we will refer to these two sets of objects as the low and high X-ray resolution samples. Furthermore, we note that whereas O'Sullivan et al. include all sort of early-type galaxies, Boroson et al. restricted themselves to well-studied X-ray objects and explicitly excluded the dominant galaxies of groups and clusters that are associated with extended hot gas haloes confined by the group or cluster gravitational potential.

For the galaxies in these two ATLAS^{3D} subsamples Paper I provides their currently best distance estimates, consistently derived values for their K-band luminosity L_K starting from 2MASS apparent magnitude, and effective radius R_e. Homogeneously derived values for the apparent ellipticity $\epsilon = 1 - b/a$ were obtained in Paper III through the analysis of the images at our disposal (mostly from the Sloan Digital Sky Survey), whereas Cappellari et al. (2013a, hereafter Paper XV) provide us with accurate dynamical mass measurement, M_{dyn}, based on the detailed Jeans anisotropic dynamical modelling (Cappellari 2008) of the stellar kinematics obtained from our Spectrographic Aerial Unit for Research on Optical Nebulae (SAURON) data.[1]

The SAURON data also allow us to probe the depth of the gravitational potential well using values for the stellar velocity dispersion σ extracted within the same physical aperture and to assess the degree of rotational support using the λ_R parameter introduced by Emsellem et al. (2007). Since we are interested in the global shape and degree of rotational support of our sample galaxies, we adopt here the values for λ_{Re} and ϵ_e that in Paper III were computed within the galaxy effective radius R_e. Similarly, as we are interested in tracing most of the potential well, we will use the stellar velocity dispersion values σ_e (also provided by Paper XV) that are extracted within an elliptical aperture of equivalent circular radius R_e. The use of ϵ in conjunction with λ_R will help us in separating face-on but intrinsically flat and fast-rotating objects from much rounder and slowly rotating galaxies, as well as in identifying galaxies that may be intrinsically quite flat also in this latter class of objects (most likely as they are triaxial in shape).

All the quantities described in this section are listed in Tables 1 and 2 for the galaxies in the low and high X-ray resolution subsamples, respectively. These tables also include rescaled X-ray luminosity values from the literature assuming the ATLAS^{3D} distance estimates, which, unless otherwise stated, will be used in our analysis.

3 RESULTS

3.1 Low X-ray resolution sample

We start this section by showing in Fig. 1 how the galaxies in the low X-ray resolution sample fare in the classic L_B–L_X diagram when using the values for the B band and X-ray luminosity taken from the catalogue of O'Sullivan et al. (2001), without any distance rescaling. The dashed and solid lines in Fig. 1 trace the expected contribution to the observed L_X from the unresolved emission of low-mass X-ray binaries, as first estimated by O'Sullivan et al. and subsequently by Kim & Fabbiano (2004). The dotted lines also show the uncertainties associated with the Kim & Fabbiano calibration, which was based on the luminosity function of LMXBs resolved

[1] More specifically, the values used here are those based on the self-consistent model (B) of Paper XV, where they are indicated as M_{JAM}. Such M_{JAM} values provide an approximation for twice the mass contained within a sphere enclosing half of the galaxy light. Given that the stars dominate the mass budget inside that sphere, M_{JAM} also provides a good estimate for the total stellar mass M_{stars} of a galaxy, while also including possible variations of the initial stellar mass function (see e.g. Cappellari et al. 2012).

Table 1. X-ray and optical properties for the galaxies of our low X-ray resolution ATLAS^{3D} subsample.

NGC (1)	$L_{B,\,OS}$ (2)	$L_{X,\,OS}$ (3)	D_{OS} (4)	D (5)	M_K (6)	L_K (7)	L_X (8)	λ_{Re} (9)	ϵ_e (10)	Fast/slow (11)	σ_e (12)	M_{dyn} (13)
2577	9.74	40.19	28.7	30.8	−23.41	10.68	40.25	0.70	0.47	F	2.293	10.921
2768	10.57	40.38	20.9	21.8	−24.71	11.20	40.42	0.25	0.47	F	2.297	11.534
2974	10.50	40.58	28.3	20.9	−23.62	10.76	40.32	0.66	0.41	F	2.355	11.133
3193	10.15	39.96	21.6	33.1	−24.63	11.16	40.33	0.19	0.13	F	2.252	11.153
3226	10.12	40.20	21.6	22.9	−23.24	10.61	40.25	0.25	0.17	F	2.183	10.993
3605	9.47	39.08	19.8	20.1	−21.83	10.04	39.09	0.43	0.41	F	1.923	10.002
3607	10.46	40.54	19.8	22.2	−24.74	11.21	40.64	0.21	0.19	F	2.315	11.342
3608	10.11	40.01	19.8	22.3	−23.65	10.77	40.11	0.04	0.19	S	2.228	10.956
3610	10.40	39.83	27.3	20.8	−23.69	10.79	39.59	0.53	0.38	F	2.260	10.744
3640	10.43	39.92	22.9	26.3	−24.60	11.15	40.04	0.38	0.19	F	2.246	11.223
3665	10.70	40.60	30.8	33.1	−24.92	11.28	40.66	0.41	0.22	F	2.335	11.556
3998	10.08	41.51	17.5	13.7	−23.33	10.64	41.30	0.45	0.17	F	2.350	10.938
4168	10.40	40.56	33.7	30.9	−24.03	10.92	40.48	0.04	0.13	S	2.232	11.300
4203	9.89	41.18	16.2	14.7	−23.44	10.69	41.09	0.31	0.15	F	2.111	10.604
4261	10.70	41.21	31.5	30.8	−25.18	11.38	41.19	0.09	0.22	S	2.424	11.722
4278	10.24	40.36	16.2	15.6	−23.80	10.83	40.33	0.18	0.10	F	2.328	11.076
4340	9.84	39.75	15.9	18.4	−23.01	10.52	39.88	0.46	0.23	F	2.027	10.566
4365	10.34	40.25	15.9	23.3	−25.21	11.40	40.58	0.09	0.25	S	2.345	11.525
4374	10.57	40.83	15.9	18.5	−25.12	11.36	40.96	0.02	0.15	S	2.412	11.585
4382	10.64	40.33	15.9	17.9	−25.13	11.36	40.43	0.16	0.20	F	2.253	11.448
4387	9.47	39.71	15.9	17.9	−22.13	10.16	39.81	0.40	0.37	F	1.998	10.182
4406	10.66	42.05	15.9	16.8	−25.04	11.33	42.10	0.05	0.21	S	2.280	11.600
4458	9.51	39.84	16.1	16.4	−21.76	10.02	39.85	0.07	0.12	S	1.947	10.032
4459	10.20	40.17	15.9	16.1	−23.89	10.87	40.18	0.44	0.15	F	2.199	10.919
4472	10.90	41.43	15.9	17.1	−25.78	11.62	41.49	0.08	0.17	S	2.398	11.775
4473	10.15	40.14	16.1	15.3	−23.77	10.82	40.09	0.23	0.42	F	2.271	10.928
4477	10.13	40.26	15.9	16.5	−23.75	10.81	40.29	0.22	0.14	F	2.173	10.943
4486	10.85	42.95	15.9	17.2	−25.38	11.46	43.02	0.02	0.04	S	2.422	11.727
4526	10.47	39.87	15.9	16.4	−24.62	11.16	39.90	0.45	0.36	F	2.320	11.243
4550	9.72	39.78	15.9	15.5	−22.27	10.22	39.76	0.10	0.65	S	2.062	10.396
4552	10.29	40.71	15.9	15.8	−24.29	11.03	40.70	0.05	0.05	S	2.351	11.202
4621	10.32	40.02	15.9	14.9	−24.14	10.97	39.96	0.29	0.37	F	2.296	11.119
4636	10.51	41.59	15.9	14.3	−24.36	11.06	41.50	0.04	0.09	S	2.259	11.396
4638	9.80	39.59	15.9	17.5	−23.01	10.52	39.67	0.69	0.61	F	2.134	10.408
4649	10.73	41.28	15.9	17.3	−25.46	11.50	41.35	0.13	0.16	F	2.428	11.719
4697	10.55	40.12	15.1	11.4	−23.93	10.88	39.87	0.32	0.45	F	2.229	11.067
4753	10.46	39.99	20.2	22.9	−25.09	11.35	40.10	0.47	0.21	F	2.241	11.388
4762	10.16	40.13	15.9	22.6	−24.48	11.10	40.43	0.72	0.85	F	2.126	11.106
5273	9.68	39.86	17.1	16.1	−22.37	10.26	39.81	0.52	0.11	F	1.824	10.249
5322	10.67	40.21	27.8	30.3	−25.26	11.42	40.28	0.07	0.31	S	2.351	11.532
5353	10.56	41.00	34.7	35.2	−25.11	11.36	41.01	0.62	0.55	F	2.449	11.503
5507	9.63	39.75	25.9	28.5	−23.19	10.59	39.83	0.50	0.25	F	2.216	10.729
5838	10.20	40.02	22.9	21.8	−24.13	10.96	39.98	0.52	0.36	F	2.350	11.157
5846	10.66	41.65	22.9	24.2	−25.01	11.32	41.70	0.03	0.06	S	2.349	11.573
5866	10.32	39.69	13.2	14.9	−24.00	10.91	39.80	0.32	0.57	F	2.196	11.001
7465	9.64	41.36	24.3	29.3	−22.82	10.44	41.52	0.28	0.36	F	1.981	10.200

Note. Column (1): NGC number. Columns (2)–(4): *B*-band luminosity, X-ray luminosity (in logarithm of $L_{B,\odot}$ and erg s^{-1}, respectively) and distance estimates (in Mpc) from O'Sullivan et al. (2001). Columns (5) and (6): distance and absolute *K*-band magnitude from table 3 of Paper I. Columns (7) and (8): *K*-band and X-ray luminosity (in logarithm of $L_{K,\odot}$ and erg s^{-1}, respectively) computed and rescaled from the values listed in columns (6) and (3), respectively, while adopting our distance estimate of column (5). Columns (9)–(11): λ_R parameter, ellipticity and fast versus slow rotator kinematic classification derived within the galaxy effective radius R_e, from table B1 of Paper III. Columns (12) and (13): stellar velocity dispersion (in km s^{-1}) and dynamical mass (in logarithm of $M_\odot$) measured within one R_e, from table 1 of Paper XV (where the adopted mass is M_{JAM}). This table is also available from our project website http://purl.org/atlas3d.

with *Chandra* images in a sample of 14 E and S0s. The other early-type galaxies with L_X detections in the O'Sullivan et al. catalogue are also plotted in Fig. 1, to illustrate better how traditionally a $L_B \sim 1$–$3 \times 10^{10}\,L_\odot$ would mark the onset of a $L_X \propto L_B^2$ trend due to the presence of a diffuse component. X-ray bright objects at low L_B values in this diagram are most likely outliers that own their X-ray flux either to a central AGN or the surrounding ICM, which should be isolated when considering the nature of the scatter in the L_X values from the hot gas. In fact, the three labelled sources in Fig. 1 were already identified by O'Sullivan et al. as powerful AGN. Fig. 1 also shows that due to the volume-limited nature of the ATLAS^{3D} sample our objects fall short from covering the entire

Table 2. X-ray and optical properties for the galaxies of our high X-ray resolution ATLAS^{3D} subsample.

NGC (1)	$L_{X,\,gas,\,B}$ (2)	D_B (3)	D (4)	M_K (5)	L_K (6)	$L_{X,\,gas}$ (7)	kT (8)	λ_{Re} (9)	ϵ_e (10)	Fast/slow (11)	σ_e (12)	M_{dyn} (13)
0821	37.33	24.1	23.4	−23.99	10.91	37.30	0.15	0.27	0.39	F	2.254	11.095
1023	38.80	11.4	11.1	−24.01	10.92	38.77	0.32	0.39	0.36	F	2.222	10.819
2768	40.10	22.3	21.8	−24.71	11.20	40.08	0.34	0.25	0.47	F	2.297	11.534
3377	38.07	11.2	10.9	−22.76	10.42	38.04	0.22	0.52	0.50	F	2.108	10.468
3379	38.67	10.5	10.3	−23.80	10.83	38.65	0.25	0.16	0.10	F	2.269	10.915
3384	38.54	11.5	11.3	−23.52	10.72	38.53	0.25	0.41	0.06	F	2.140	10.564
4261	40.85	31.6	30.8	−25.18	11.38	40.82	0.66	0.09	0.22	S	2.424	11.722
4278	39.42	16.0	15.6	−23.80	10.83	39.40	0.32	0.18	0.10	F	2.328	11.076
4365	39.71	20.4	23.3	−25.21	11.40	39.82	0.44	0.09	0.25	S	2.345	11.525
4374	40.77	18.3	18.5	−25.12	11.36	40.78	0.63	0.02	0.15	S	2.412	11.585
4382	40.08	18.4	17.9	−25.13	11.36	40.05	0.40	0.16	0.20	F	2.253	11.448
4472	41.28	16.2	17.1	−25.78	11.62	41.32	0.80	0.08	0.17	S	2.398	11.775
4473	39.27	15.7	15.3	−23.77	10.82	39.24	0.35	0.23	0.42	F	2.271	10.928
4526	39.52	16.9	16.4	−24.62	11.16	39.49	0.33	0.45	0.36	F	2.320	11.243
4552	40.36	15.3	15.8	−24.29	11.03	40.39	0.52	0.05	0.05	S	2.351	11.202
4621	38.78	18.2	14.9	−24.14	10.97	38.61	0.27	0.29	0.37	F	2.296	11.119
4649	41.07	16.8	17.3	−25.46	11.50	41.09	0.77	0.13	0.16	F	2.428	11.719
4697	39.28	11.7	11.4	−23.93	10.88	39.26	0.33	0.32	0.45	F	2.229	11.067
5866	39.38	15.3	14.9	−24.00	10.91	39.36	0.35	0.32	0.57	F	2.196	11.001

Note. Column (1): NGC number. Columns (2) and (3): hot gas X-ray luminosity (in logarithm of erg s^{-1}) and distance estimates (in Mpc) from Boroson et al. (2011). Columns (4) and (5): distance and absolute *K*-band magnitude from table 3 of Paper I. Columns (6) and (7): *K*-band and hot gas luminosity (in logarithm of $L_{K,\odot}$ and erg s^{-1}, respectively) computed and rescaled from the values listed in columns (5) and (2), respectively, while adopting our distance estimate of column (4). Column (8): hot gas temperature (in keV), from Boroson et al. Columns (9)–(11): λ_R parameter, ellipticity and fast versus slow rotator kinematic classification derived within the galaxy effective radius R_e, from table B1 of Paper III. Columns (12)–(13) stellar velocity dispersion dynamical mass (in logarithm of km s^{-1} and $M_\odot$, respectively) measured within one R_e, from table 1 of Paper XV (where the adopted mass is M_{JAM}). This table is also available from our project website http://purl.org/atlas3d.

range of optical luminosity spanned by the sample of O'Sullivan et al., although only by a factor of 2.

We now move on from this first diagram and start making use of our ATLAS^{3D} data base by considering in Fig. 2 the near-infrared *K*-band luminosity of our sample galaxies, which corresponds much more closely to the total stellar mass than does the *B*-band optical luminosity, in particular in the occasional presence in early-type galaxies of a younger stellar subcomponent. Furthermore, in Fig. 2 we now adopt the currently best estimates for the distance of our sample galaxies, not only to compute the L_K luminosity from the 2MASS apparent *K*-band magnitudes but also to rescale the L_X values given in O'Sullivan et al. Compared to Fig. 1, in the L_K–L_X diagram the bright galaxies with the largest X-ray luminosities appear to distance themselves more from other objects with L_X exceeding the value expected from discrete sources. All such galaxies are either deeply embedded in the ICM of the Virgo cluster (NGC 4486 and NGC 4406) or are the central member of their own group of galaxies and show a rather extended X-ray halo (NGC 4636 and NGC 5846; Matsushita 2001; Mulchaey et al. 2003; Santos, Mendes de Oliveira & Sodré 2007). This suggests that the ICM contributes largely to the L_X values of these objects, which should then be flagged in the remainder of our analysis as in the case of the AGN identified above. We also note that in the L_K–L_X diagram L_K is a more accurate predictor for the contribution of LMXBs to the total L_X values, although whether most or just a few of our sample objects could be considered to possess an X-ray halo still depends, like in Fig. 1, on the adopted calibration for the L_X from LMXBs. Yet, the Kim & Fabbiano (2004) calibration appears problematic since according to it there would appear to be a considerable fraction of galaxies in the L_K–L_X diagram whose L_X values are nearly half what would be expected from LMXBs alone. The more recent calibration of Boroson et al. (2011) does not suffer from this bias, which is why we will adopt it throughout the rest of our analysis.

To further understand the nature of the L_X emission in our sample galaxies, in Fig. 3 we have placed them in the $L_K\sigma_e^2$ versus L_X diagram. This is a near-infrared and integral-field version of the $L_B\sigma^2$ versus L_X diagram introduced by Canizares et al. (1987), where the combination of L_K and σ_e allows to trace the X-ray luminosity that is expected if the energy lost by the hot gas through radiation is compensated by the thermalization of the kinetic energy that the stellar ejecta inherit from their parent stars. Such an input rate of kinetic energy L_σ would indeed correspond to the stellar mass loss rate $\dot{M}$ (traced by L_K) times the specific kinetic energy associated with the stellar random motions (traced by σ_e^2). More specifically, we take $L_\sigma = \frac{3}{2}\dot{M}\sigma_e^2$. To show the prediction of such a model in Fig. 3 we computed the average ratio between the *K*- and *B*-band luminosity of our sample galaxies ($\log L_K/L_B = 0.7$) and assumed a mass-loss rate $\dot{M}$ of $1.5 \times 10^{-11}(L_B/L_\odot)t_{15}^{-1.3}\,M_\odot\,yr^{-1}$ (as given by Ciotti et al. 1991) with an average stellar age t_{15} (in units of 15 Gyr) of 12 Gyr. By adding to this model the expected contribution $L_{X,\,discr}$ from the unresolved LMXB population according to the calibration of Boroson et al., which we plotted in the $L_K\sigma_e^2$–L_X diagram using the best-fitting near-infrared Faber–Jackson correlation (Faber & Jackson 1976) between the L_K and σ_e values for our low X-ray resolution sample ($\log\sigma_e = 0.285\log L_K - 0.864$), we finally obtain the total L_X values that ought to be compared with the data shown in Fig. 3.

Incidentally, except for two objects, all the slowly rotating galaxies in our low X-ray resolution sample that are massive enough to heat up the stellar loss material at X-ray temperatures and lead

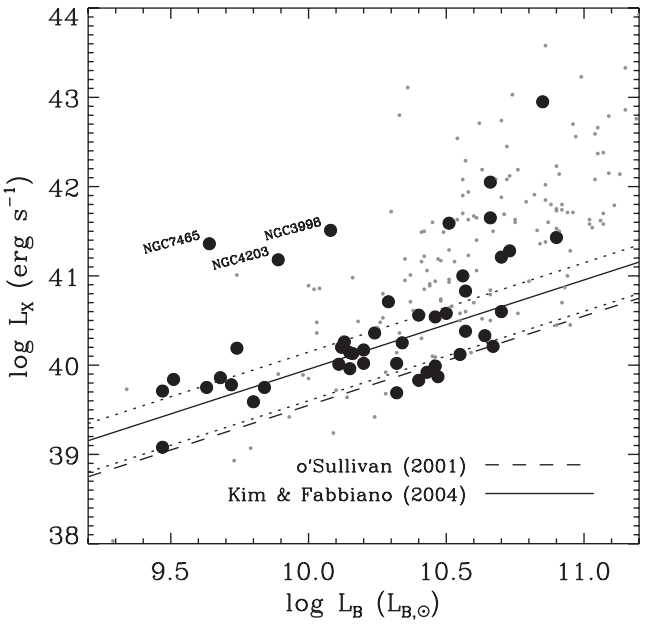

Figure 1. L_B versus L_X of our low X-ray resolution ATLAS^{3D} subsample galaxies, based on luminosity and distance values from the literature and essentially (except for one object) from O'Sullivan et al. (2001). The dashed and solid lines trace the expected contribution to the observed L_X from the unresolved emission of low-mass X-ray binaries, as estimated by O'Sullivan et al. and Kim & Fabbiano (2004), respectively. The dotted lines show the uncertainties associated with the Kim & Fabbiano calibration. The three labelled sources, already identified by O'Sullivan et al., owe most of their X-ray flux to the presence of strong nuclear activity. The small grey dots show the other early-type galaxies with detected L_X values in the catalogue of O'Sullivan et al.

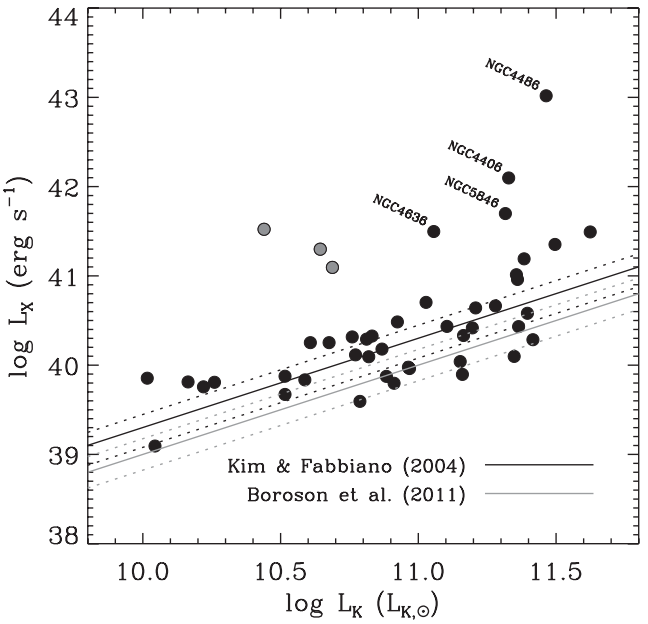

Figure 2. L_K versus L_X of our low X-ray resolution ATLAS^{3D} subsample galaxies, now based on luminosity values obtained adopting our own compilation of distance values. The solid and dotted lines trace the expected contribution to the observed L_X values, with uncertainties, from the unresolved emission of low-mass X-ray binaries, as given by Kim & Fabbiano (2004) in black and by Boroson et al. (2011) in grey. In this diagram, the labelled objects with the largest X-ray luminosities are either deeply embedded in the ICM of the Virgo cluster (NGC 4486, NGC 4406) or are the central member of their own group of galaxies and show a rather extended X-ray halo (NGC 4636, NGC 5846). Grey symbols show the objects with AGN that were identified in Fig. 1.

to detectable X-ray luminosities against the LMXBs background (in Fig. 3 we considered a generous lower limit for $\log L_K \sigma_e^2$ of $14.6\,L_{K,\odot}\,km^2\,s^{-2}$, corresponding to $M_{dyn} \gtrsim 2 \times 10^{10}\,M_\odot$) align themselves along the lines of such a simple model, falling either directly on top or just above the predicted L_X values. We note that a situation where the radiation losses of the hot atmosphere are balanced by the thermalization of the kinetic energy of the stellar ejecta would implicitly require that the stellar mass loss material is steadily removed from the galaxy, in order the prevent the accumulation of gas and catastrophic cooling. For a typical old and massive early-type galaxy such a quasi-static situation could be maintained by Type Ia SNe explosions, since at their present-day rate the SNe energy output L_{SN} is comparable to the energy L^-_{grav} that is necessary to extract the stellar mass material (see e.g. the spherical test case of Pellegrini 2012, with a $L_B = 5 \times 10^{10} L_B$ that would correspond to $\log L_K \sigma_e^2 \sim 16.2$).

On the other hand, most of the fast-rotating galaxies in this sample fall short of the X-ray luminosity expected from stellar ejecta that through shocks and collisions contribute to heat the hot gas. If we consider the early finding of Eskridge et al. (1995a,b) that S0s and flat Es have a lower X-ray luminosity compared to rounder elliptical of similar optical luminosity, and that when early-type galaxies are split by their degree of rotational support 94 per cent of S0s and 66 per cent of Es fall in the fast-rotating category (Paper III), then it seems natural to ask whether the apparent X-ray deficiency observed in Fig. 3 for this class of objects is actually driven by the λ_R parameter or by the apparent flattening ϵ.

For the objects in our low X-ray resolution ATLAS^{3D} subsample, Fig. 4 shows how the ratio of their total X-ray luminosity L_X to the expected contribution from unresolved discrete sources only $L_{X,\,discr}$ or to the predicted X-ray luminosity when including also the emission from stellar mass loss material heated to the stellar kinetic temperature $L_{X,\,discr\,+\,diff}$ correlates with the λ_{Re} parameter, apparent flattening ϵ_e and dynamical mass M_{dyn}. A Spearman rank analysis reveals that both the $L_X/L_{X,\,discr}$ and $L_X/L_{X,\,discr\,+\,diff}$ ratios correlate with a modest degree of significance with both λ_{Re} and ϵ_e (see Fig. 4 for the probability of the null hypothesis for each correlation). The $L_X/L_{X,\,discr}$ excess would appear to be also somehow correlated to the dynamical mass M_{dyn}, although no such trend is observed in the case of the $L_X/L_{X,\,discr\,+\,diff}$ deficit. In other words, pretty much independently of their dynamical mass, increasingly rounder and more slowly rotating galaxies in our low X-ray resolution ATLAS^{3D} subsample appear to show also larger L_X values that progressively exceed what is expected from the LMXB population and eventually become consistent with the total predicted X-ray luminosity from LMXBs and shock-heated stellar ejecta. Conversely, the flatter and more rotationally supported a galaxy, the larger its L_X deficit from the expectation of this simple model.

The most notable outliers from the trends observed in Fig. 4 not only support this interpretation of the data but also appear to suggest that the intrinsic flattening of a galaxy, rather than its degree of rotational support, is what really drives the L_X deficiency of fast rotators. When considering the correlations between ϵ_e and either $L_X/L_{X,\,discr}$ or $L_X/L_{X,\,discr\,+\,diff}$, which are the most significant in Fig. 4, we note that three of the roundest galaxies (NGC 3193, NGC 3640 and NGC 4753) are likely to be intrinsically flat objects that are viewed face-on, which would move to the right of the central panels of Fig. 4 if seen from a less improbable angle.

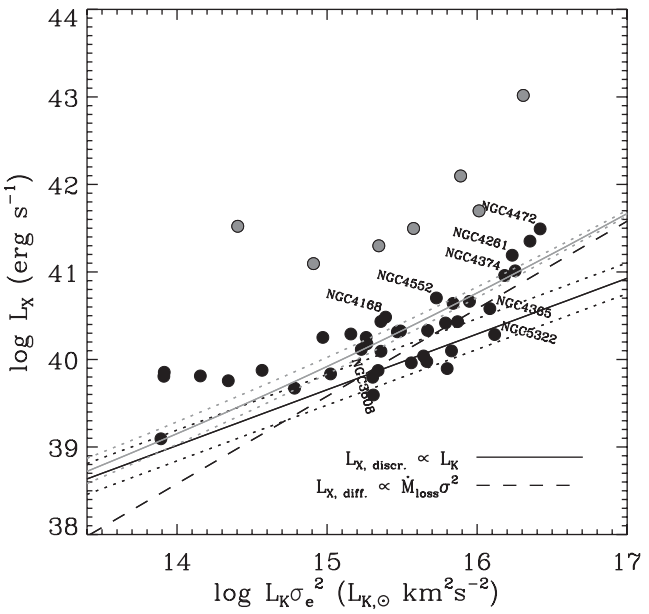

Figure 3. $L_K\sigma_e^2$ versus L_X diagram for our low X-ray resolution ATLAS^{3D} subsample galaxies, to check whether their diffuse hot gas luminosity can be explained in terms of stellar mass loss material that through shocks and collisions thermalized the kinetic energy inherited by their parent stars. The prediction of such a model, whereby $L_{X,diff} = L_\sigma = \frac{3}{2}\dot{M}\sigma_e^2$, is shown by the dashed line, whereas the contribution (with uncertainties) of unresolved X-ray binaries ($L_{X,\,discr}$, according to Boroson et al. 2011) is shown by the solid and dotted lines (see text for more details on both components). Finally, the grey solid and dashed lines show the sum of both diffuse and discrete components, which is what we expect to observe in the absence of strong AGN or ICM contamination. Beside two exceptions, all the slowly rotating galaxies in our low X-ray resolution sample that are massive enough to heat up the stellar loss material to X-ray-emitting temperatures (labelled objects) lie directly on top of above the prediction of such a simple model, whereas most fast rotators fall short of this benchmark. Grey symbols indicate either objects with AGN or that are deeply embedded in their group or cluster medium, as shown in Figs 1 and 2.

This is supported by their large values for λ_{Re}, which indicates that they are in fact rotationally supported systems just like all the other fast rotators with which they share the trends with λ_{Re} that is observed in the left-hand panels of Fig. 4. Conversely, in these same panels, the only slow rotators with L_X values consistent with just emission from LMXBs or that fall short of the predicted total L_X from LMXBs and hot gas sustained by the thermalization of the kinetic energy of stellar ejecta, NGC 4365 and NGC 5322, are incidentally the flattest objects among the class of slow rotators. In fact that these (fairly massive) objects appear to align themselves with the rest of the fast rotators in the anticorrelations between the apparent flattening ϵ_e and either $L_X/L_{X,\,discr}$ or $L_X/L_{X,\,discr+diff}$ further suggests that it is their intrinsic shape, rather than their dynamical state, which determines whether they are capable to retain a halo of hot gas. When such flat slow rotators are excluded from the Spearman rank analysis the correlations involving λ_{Re} in Fig. 4 become more significant, and the same holds when excluding the face-on fast rotators from the correlations involving ϵ_e. Finally, we note that even a modest contamination from a central AGN or the intragroup or -cluster medium to the total X-ray in the least massive objects could significantly impact on the total L_X values for these object. In turn, this would generally weaken the significance of any correlation between λ_{Re} or ϵ_e and the $L_X/L_{X,\,discr}$ or $L_X/L_{X,\,discr+diff}$ ratios, since low-mass galaxies generally tend to be fast rotators (Paper III). The possible impact of AGN or the intragroup or -cluster medium is most noticeable in the correlation between λ_{Re} and the $L_X/L_{X,\,discr+diff}$ deficit (lower left-hand panel of Fig. 4), where the majority of the most rotationally supported galaxies with $L_X/L_{X,\,discr+diff}$ values near unity have $\log L_K\sigma_e^2$ values below of $15.4\,L_{K,\odot}\,km^2\,s^{-2}$. At such a low $\log L_K\sigma_e^2$ regime the typical AGN X-ray emission $L_{X,\,AGN}$ of early-type galaxies could be comparable to the predicted values for $L_{X,\,discr}$ and $L_{X,\,diff}$ (Fig. 3). For instance, the median $L_{X,\,AGN}$ value for the ATLAS^{3D} sample galaxies that appear in the study of Liu (2011, 42 objects) is $2.6\times10^{39}\,erg\,s^{-1}$.

To summarize the results of this subsection, in Fig. 5 we redraw the same L_K–L_X and $L_K\sigma_e^2$–L_X diagrams presented in Figs 2 and 3, but now with elliptical symbols coded by colour and flattening according to the values of λ_{Re} and the ϵ_e of the galaxies they are representing. This is done in order to convey more visually our preliminary conclusion, based on our low X-ray resolution sample, that only round slow rotators can sustain a halo of hot gas from the thermalization of the kinetic energy carried by their stellar mass loss material whereas fast rotators (and apparently also flat slow rotators) have progressively fainter X-ray haloes the flatter and more rotationally supported they appear.

3.2 High X-ray resolution sample

The previous conclusions on the more limited ability of fast-rotating, or even more generally just flat, early-type galaxies to retain their haloes of hot gas have to be taken with care given that they are based on X-ray data of rather coarse spatial resolution where the contribution from a central AGN, the intragroup or -cluster medium or LMXBs to the total L_X values can only be estimated, and which in the case of LMXBs is known to be the subject of considerable scatter.[2] It is therefore important to ask whether our results hold when such factors can be properly isolated through the use of *Chandra* or *XMM*.

Recently, Boroson et al. (2011) published one of the largest samples of early-type galaxies with consistently derived $L_{X,\,gas}$ measurements, which overlaps well with the ATLAS^{3D} sample and excludes the dominant members of groups and clusters of galaxies. For the objects that we have in common with the sample of Boroson et al., Fig. 6 shows how their $L_K\sigma_e^2$ and $L_{X,\,gas}$ values compare to each other, thus allowing to directly check whether the hot gas luminosity corresponds to the input rate of kinetic energy from stellar mass loss. The use of the same colour coding and squashing of Fig. 5 for our data points makes it easy to appreciate in Fig. 6 that, except for one, all the slow rotators in this ATLAS^{3D} subsample agree still remarkably well with the same simple prediction for $L_{X,\,diff} = L_\sigma$ (Fig. 3 and right-hand panel in Fig. 5). Fast rotators, on the other hand, display $L_{X,\,gas}$ values that fall systematically short of such $L_{X,\,diff}$ expected values, as does also NGC 4365, which is the flattest slow rotator in the high X-ray resolution sample and was also a lowlier compared to the rest of the slow rotators in Fig. 5 (for a more detailed picture of this galaxy, see also Davies et al. 2001; Statler et al. 2004; van den Bosch et al. 2008).

[2] If we consider that globular clusters (GCs) may be the birthplace of the LMXB population in galaxies (e.g. Sarazin, Irwin & Bregman 2000; White, Sarazin & Kulkarni 2002; Zhang, Gilfanov & Bogdan 2012) and that in turn lenticular galaxies may have a lower specific frequency S_N of GCs than elliptical galaxies (Kundu & Whitmore 2001a,b), it may be even possible that a systematically smaller number of LMXBs in fast rotators contributes to their lower X-ray luminosity. Nearly all (94 per cent) S0 galaxies and most (66 per cent) Es belong in fact to the class of fast-rotating galaxies (Paper III).

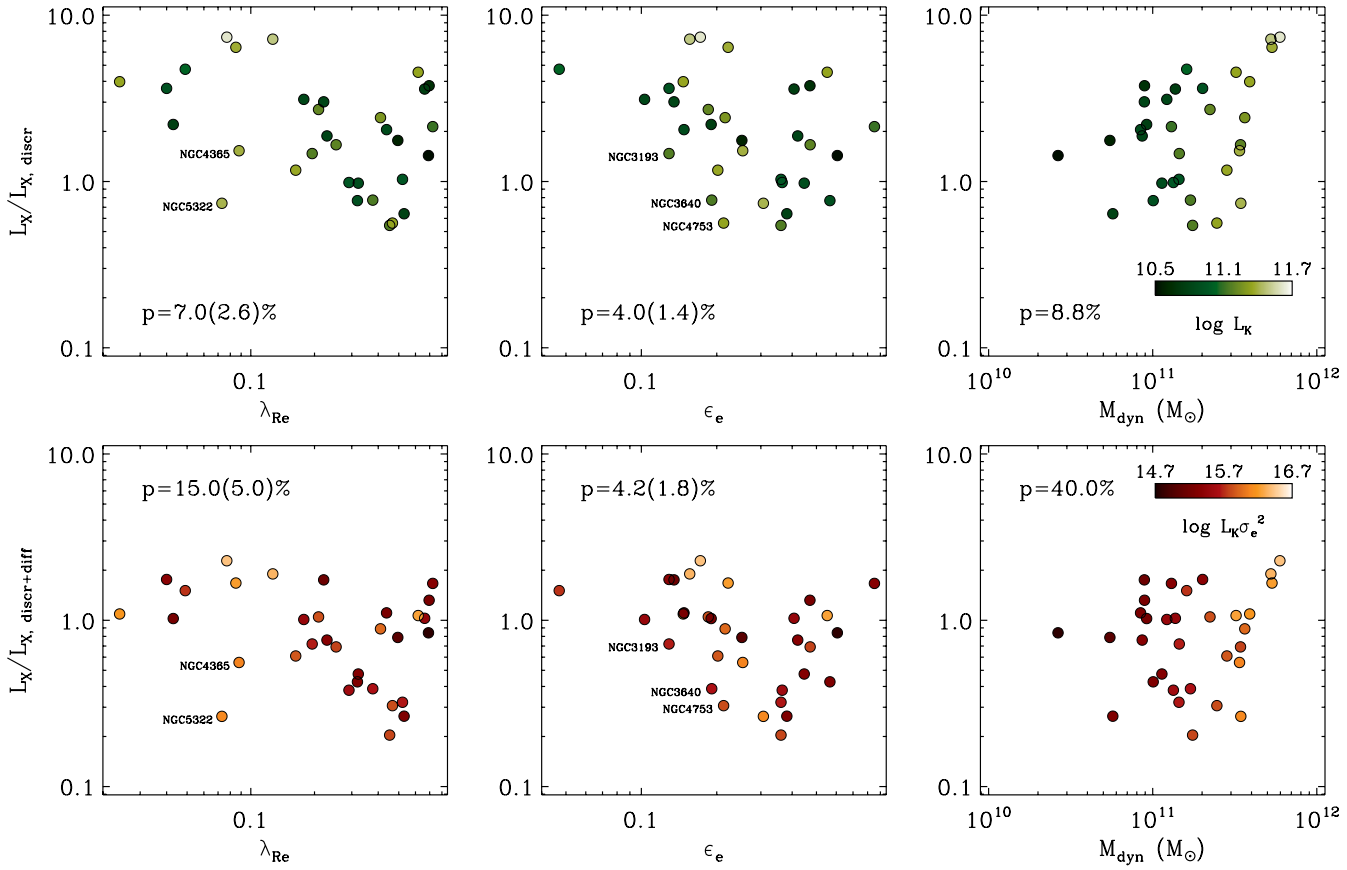

Figure 4. Correlations between the observed specific angular momentum (quantified by the λ_{Re} parameter, left-hand panels), the apparent flattening (ϵ_e, middle panels) and the dynamical mass (M_{dyn}, right-hand panels) of our low X-ray resolution ATLAS^{3D} subsample galaxies and the ratio of their total X-ray luminosity L_X to the expected contribution from unresolved discrete sources only ($L_{X,\ discr}$, upper row) or to the predicted X-ray luminosity when including also the emission from stellar mass loss material heated to the kinetic temperature of the stars ($L_{X,\ discr\ +\ diff}$, lower row). In the top and lower panels the symbols are colour coded according to the total K-band luminosity L_K and the value of $L_K\sigma_e^2$ for our sample galaxies, respectively, in order to trace their position in Figs 2 and 3. Objects with $\log L_K\sigma_e^2 \leq 14.6\,L_{K,\odot}\ km^2\ s^{-2}$, which would not be sufficiently massive to sustain a detectable X-ray halo against the LMXBs background, and NGC 3226, whose L_X value is contaminated by the presence of the nearby active galaxy NGC 3227, are not shown. Excluding these galaxies, each panel shows the values of the Spearman test probability p of the null hypothesis whereby the plotted quantities would follow each other monotonically (not necessarily linearly) only by mere chance. Values within parentheses refer to p values computed while excluding the labelled objects in the corresponding panels.

If Fig. 6 already seem to supports the picture that was drawn in Section 3.1 using *ROSAT* or *Einstein* data, Fig. 7 further confirms that the X-ray deficiency of fast rotators, as quantified by the $L_{X,\ gas}/L_{X,\ diff}$ ratio, correlates indeed with their degree of rotational support traced by the λ_{Re} parameter and apparent flattening ϵ_e. The connection with λ_{Re} in particular is remarkably significant given the modest number of objects at our disposal, and the general trend in the left-hand panel of Fig. 7 can be recognized also in the lower left-hand panel of Fig. 4 that showed the correlation between λ_{Re} and the $L_X/L_{X,\ discr\ +\ diff}$ deficit for our low X-ray resolution sample, if one were to disregard (with the benefit of hindsight) the least massive fast rotators. The behaviour of the outliers to the present correlations with λ_{Re} and ϵ_e is also similar to what is observed in Fig. 4, with the flat slow rotator NGC 4365 falling below the main trend between $L_{X,\ gas}/L_{X,\ diff}$ and λ_{Re} but aligning itself with the majority of the fast rotators in the $L_{X,\ gas}/L_{X,\ diff}$ versus ϵ_e diagram and with a few round fast rotators (NGC 3384, NGC 4278 and NGC 3379) acting in the opposite way, which adds to the idea that the ability of a galaxy to retain a halo of hot gas relates primarily to its intrinsic shape (Ciotti & Pellegrini 1996; D'Ercole & Ciotti 1998). In fact, that the correlation between the $L_{X,\ gas}/L_{X,\ diff}$ ratio and λ_{Re} is more significant than in the case of the correlation with ϵ_e suggests that λ_{Re} may be a good indicator for the intrinsic flattening of fast rotators, if this is indeed the main parameter driving the X-ray deficit.

It is interesting to observe in the right-hand panel of Fig. 7 how the direct $L_{X,\ gas}$ measurements derived from the *Chandra* data now reveal that the dynamical mass M_{dyn} must also play a role in determining how much hot gas a galaxy can retain. This is not unexpected, since the ratio of the energy that could be injected by Type Ia SN in the interstellar medium L_{SN} and the energy required to steadily extract the mass lost by stars L_{grav}^{-} in itself depends on the galaxy mass, so that the less massive galaxies would host SN-driven outflows and thus possess systematically less massive and X-ray fainter hot gas atmospheres. In principle, it may be even possible that the correlation with between λ_{Re} and $L_{X,\ gas}$ is partly driven by the correlation with M_{dyn}, since low rotators tend to be more massive then fast rotators (Paper III). Yet, a large M_{dyn} appears to be only a necessary, but not sufficient condition for having a bright X-ray halo. Almost all fast rotators in our high X-ray resolution sample are nearly as massive, within a factor of 2, as the slow rotator NGC 4552 and yet they all display considerably smaller $L_{X,\ gas}$ values. Conversely, the flat slow rotator NGC 4365

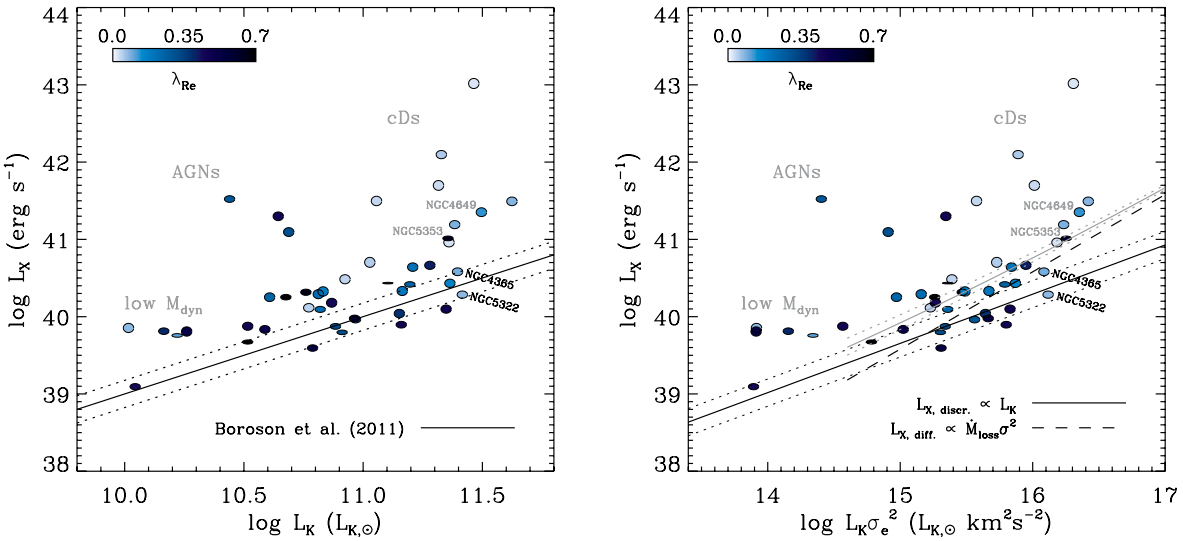

Figure 5. Same as Figs 2 and 3, but now with elliptical symbols coded by colour and flattening according to the degree of rotational support and the apparent ellipticity of the galaxies they are representing, in order to visually convey the dependence of the scatter in their total X-ray luminosity on these two physical parameters, as quantified in Fig. 4. The grey labels indicate the galaxies that were excluded from the analysis of the correlation presented in Fig. 4. The other galaxies labelled on the left- and right-hand panels are, respectively, most likely face-on but intrinsically flat and rotationally supported galaxies and the flattest slow rotators in our low X-ray resolution ATLAS^{3D} subsample. Finally, in both panels we also label in grey the two most massive X-ray bright fast rotators, NGC 4649 and NGC 5353. The kinematic classification of NGC 4649 is somehow uncertain, however, since this object lies almost exactly on the dividing line between fast and slow rotators defined in Paper III, whereas the very flat NGC 5353 happens to be the most massive member of the compact group of galaxies HCG 68, so that its total L_X may also include emission from hot gas confined by the group potential.

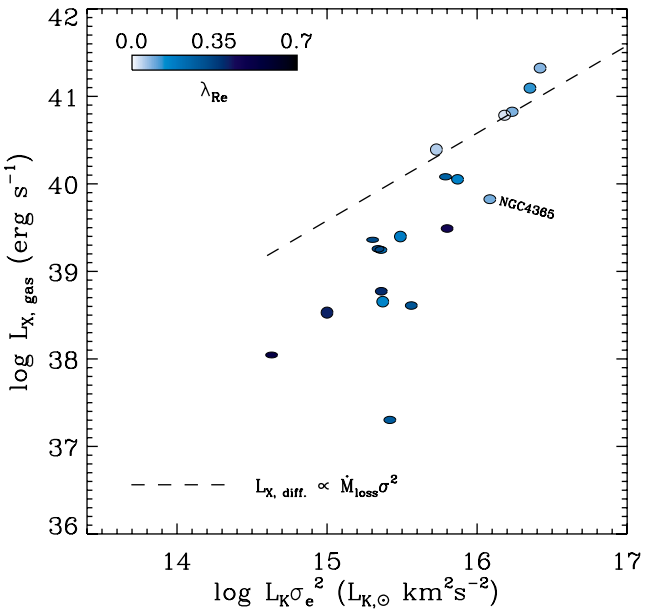

Figure 6. $L_K\sigma_e^2$ versus $L_{X,\,gas}$ diagram for our high X-ray resolution ATLAS^{3D} subsample galaxies. By showing the X-ray luminosity $L_{X,\,gas}$ due only to the hot gas, this diagram checks more directly than Fig. 3 whether the X-ray haloes of the objects in our high X-ray sample originate from stellar ejecta that through shocks and collisions were heated up at X-ray emitting temperatures. The use of the same colour coding and squashing of Fig. 5 for our data points makes it easy to appreciate that, except for one, all the slow rotators in this ATLAS^{3D} subsample agree remarkably well with the same simple prediction for $L_{X,\,diff} = L_\sigma$ that was already shown in Fig. 3 and the right-hand panel of Fig. 5. Fast rotators, on the other hand, display $L_{X,\,gas}$ values that fall systematically short of the predicted values of $L_{X,\,diff}$, as does also NGC 4365, which is the flattest slow rotator in the high X-ray resolution sample.

shares with the flat rotators of our sample a relatively faint hot gas halo despite being more massive, by up to an order of magnitude, than nearly all of them.

We should also stress that the $L_{X,\,gas}/L_{X,\,diff}$ deficiency does not correlate with any of the indicators for the environmental galactic density that were adopted in Paper VII, which also confirms that the impact the ICM or group medium in our high-resolution X-ray sample has been properly avoided by following the selection of Boroson et al.

Boroson et al. (2011) also provide estimates for the hot gas temperature T, which we can use to further test whether stellar motions are the main heat source for the X-ray emitting gas (see e.g. Pellegrini 2011). If this is the case, the gas temperature should relate to the stellar velocity dispersion since this traces the stellar kinetic energy. Traditionally kT has been compared to $\mu m_p\sigma^2$ where μm_p is the mean particle mass of the gas (m_p is the proton mass and $\mu = 0.62$ for solar abundance) and σ was taken as the central stellar velocity dispersion, although T should relate more strictly to the stellar density weighted average of the intrinsic, three-dimensional velocity dispersion across the entire galaxy. Rather than venturing directly in the construction of the stellar dynamical models needed to properly evaluate this quantity, in Fig.8 we plot the kT values from Boroson et al. against our integral field measurements for the stellar velocity dispersion within one effective radius σ_e, which should already fare better than the central σ in tracing the global stellar kinetic energy.[3] In fact, by adopting the $\lambda_{Re} = 0.31\sqrt{\epsilon_e}$

[3] Pellegrini (2011) shows that the kinetic temperature associated with the stellar motions can be expressed more generally as $T_\star = \mu m_p\sigma^2\Omega/k$, where Ω relates to the dark matter fraction and to the shape of both the stellar and dark matter density radial profiles. Ω is always <1 and typically range between $\sim$0.6 and $\sim$0.8 (see fig. 2 of Pellegrini 2011). This would include the value that the σ_e^2/σ^2 ratio would take if the central σ is measured within one-eighth of the effective radius R_e (i.e. 0.76, according to equation 1 of

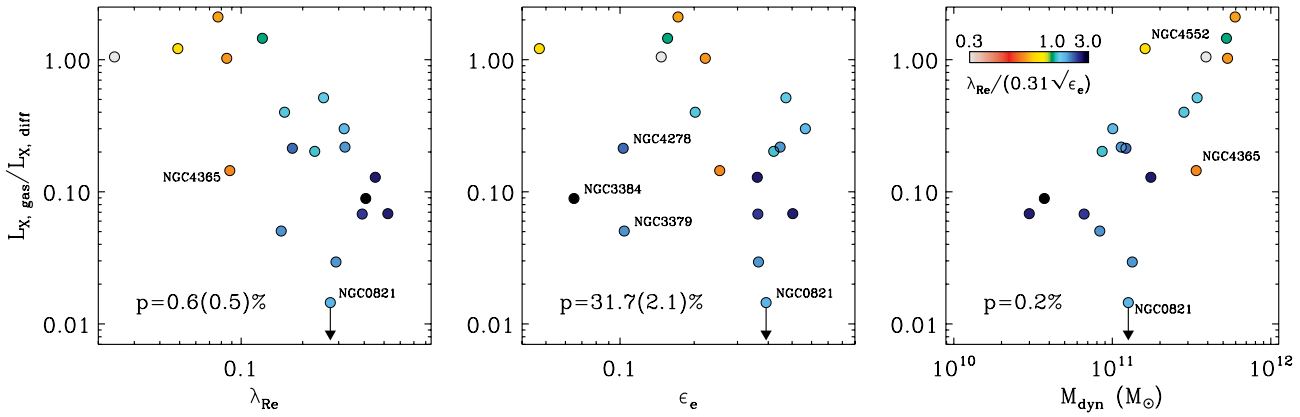

Figure 7. Correlations between the observed specific angular momentum (quantified by the λ_{Re} parameter, left), the apparent flattening ϵ_e (middle) and the dynamical mass M_{dyn} (right) of our high X-ray resolution ATLAS^{3D} subsample galaxies and their value for the ratio of the hot gas luminosity $L_{X,\,gas}$ to the X-ray luminosity $L_{X,\,diff} = L_\sigma$ that is expected in the case of stellar mass loss material heated to the kinetic temperature of the stars. As in Fig, 4, the significance of the correlation between the quantities plotted in each panel is indicated by the values of the Spearman null hypothesis probability p, which were computed while excluding the exceptionally X-ray underluminous galaxy NGC 821 (together with the labelled objects in the left-hand and central panels in order to obtain the values of p within parentheses). Here the symbols are colour coded according to their distance from the $\lambda_{Re} = 0.31\sqrt{\epsilon_e}$ dividing line between fast and slow rotators in the λ_R versus ϵ diagram (see fig. 7 of Paper III), with values for these quantities computed within R_e. Fast and slow rotators have λ_R values above and below this threshold, respectively. The $\lambda_{Re}/(0.31\sqrt{\epsilon_e})$ ratio anticorrelates with the $L_{X,\,gas}/L_{X,\,diff}$ deficit as significantly as λ_{Re} or M_{dyn}, with a null hypothesis probability $p = 0.3$ per cent (or 0.1 per cent without NGC 4365).

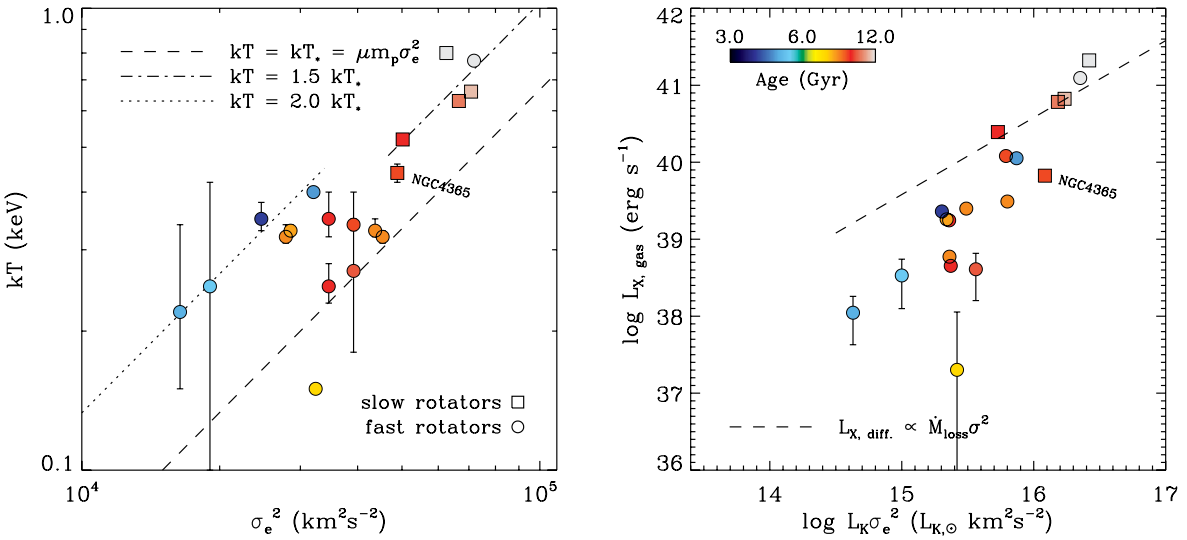

Figure 8. Left: the hot gas temperature kT of the objects in our high X-ray resolution ATLAS^{3D} subsample (from Boroson et al. 2011) against the square of their stellar velocity dispersion measured within one effective radius, σ_e. Square and round symbols indicate slow and fast rotators, respectively, and according to the $\lambda_{Re} = 0.31\sqrt{\epsilon_e}$ dividing line introduced in Paper III, whereas the colour coding traces the average stellar age of our subsample galaxies (from McDermid et al., in preparation), again within one R_e. The dashed line indicates the expected temperature if the stellar motions are the main heat source for the hot gas. The kT values of slow rotators appear consistent with such a scenario, albeit while allowing for an extra ∼50 per cent energy input (shown by the dashed–dotted line). Fast rotators, on the other hand, show similar kT values between 0.25 and 0.35 keV across a range of σ_e^2 values, although the youngest objects appear to show systematically larger temperature values (by a factor of 2, dotted line). Right: same $L_K\sigma_e^2$ versus $L_{X,\,gas}$ diagram as Fig. 6, but now using the same symbols and colour coding as in the left-hand panel in order to illustrate how the youngest fast rotators may also have brighter X-ray haloes. The position of the flat slow rotator NGC 4365 is indicated in both panels to show that despite being X-ray underluminous, this galaxy appears to display a hot gas temperature well in line with the rest of the objects in its kinematic class. The kT estimate for NGC 821 (yellow point) is very uncertain, and errors are not shown for clarity. The most massive fast rotator in both panels is again NGC 4649, whose uncertain kinematic classification was noticed in Fig. 5.

dividing line between fast and slow rotators introduced in Paper III, we note in Fig. 8 that the hot gas temperature of the slow rotators in our high X-ray resolution subsample correlates well with σ_e^2, with kT values that are on average above $\mu m_p \sigma_e^2$ by 50 per cent. On the other hand this does not seem to be the case for fast rotators, which, with the exception of the particularly cold and underluminous X-ray halo of NGC 821, show similar kT values between 0.25 and 0.35 keV across a range of σ_e^2 values and where $\mu m_p \sigma_e^2$ seems to constitute just a lower limit for the temperature of the hot gas.

Cappellari et al. 2006), as is often the case in the literature. $\mu m_p \sigma_e^2/k$ is therefore a good approximation for $T_\star$, just as it can be shown to be for $\frac{3}{2}\dot{M}\sigma_e^2$ in the case of L_σ.

As already pointed out by Pellegrini (2011), the kT excess of slow rotators could be interpreted as a need for an extra source of heating, possibly due to inflowing and adiabatically compressed gas in the central regions of these objects, which would be consistent with this kT excess being itself proportional to σ_e^2. Yet, adding an extra heat source for the gas may not seem strictly necessary given that the thermalization of the stellar kinetic energy can already account for the observed X-ray luminosity (see Fig. 6 and the right-hand panel of Fig. 8). In fact, the agreement between the observed L_X values and those traced by $L_K\sigma_e^2$ could be easily maintained even if we were to scale up the kinetic energy traced by σ_e^2 by simply considering a smaller value for the stellar mass rate $\dot{M}$, as indicated for instance by the observations of Athey et al. (2002) who give $\dot{M} = 0.8 \times 10^{-11}(L_B/\mathrm{L}_\odot)\,\mathrm{M}_\odot\,\mathrm{yr}^{-1}$ rather than the rate of $\dot{M} = 1.5 \times 10^{-11}(L_B/\mathrm{L}_\odot)\,\mathrm{M}_\odot\,\mathrm{yr}^{-1}$ that we currently adopt from Ciotti et al. (1991).

Why fast rotators do not follow the same σ_e^2–kT relation of slow rotators and instead scatter in the 0.25–0.35 keV interval is more difficult to understand. One possibility is that in fast rotators σ_e^2 may not trace particularly well the intrinsic luminosity-weighted velocity dispersion that would relate to the relative velocity involved in those shocks between stellar ejecta that are supposed to thermalized the kinetic energy inherited the stellar mass loss material, in particular since σ_e^2 measures the total kinematic broadening within one R_e and thus factors in also the impact of net rotation. On the other hand, the hot gas of fast rotators may be in an altogether different dynamical state compared to slow rotators, being most likely outflowing due to their flattening (Ciotti & Pellegrini 1996) or even driven out in a supersonic wind powered by an additional number of SNe associated with a recently formed population of stars. If gravitational heating associated with inflows is the reason why slow rotators lie above the $kT = \mu m_p \sigma_e^2$ line, then the possible absence of inflows in fast rotators may explain why a good fraction of them appear to fall close to this limit. On the other hand, the colour coding of the symbols in Fig. 8 according to their global age (within one R_e, from McDermid et al., in preparation) points to an extra input of energy from SNe as the reason why another good fraction of fast rotators display kT values well above what is expected from their σ_e^2 (by a factor of 2), since most of these objects show the presence of young populations. The right-hand panel of Fig. 8 shows that such younger objects seem also to show brighter X-ray haloes compared to older fast rotators, although more low-mass systems would certainly be needed to confirm this impression. Finally, as already pointed out by Kormendy et al. (2009), we note that a hot atmosphere would prevent also the settling of cold gas and star formation in the nuclear regions, thus preserving the distinction between galaxies with central cores and power-law surface-brightness profiles.

At this point, we should also contemplate the possibility that the kinetic energy inherited by the stellar mass loss material is not thermalized with the same efficiency in slow and fast rotators, in particular if we consider that this process is supposed to happen through shocks as the ejecta collide with each other or interact with an already existing hot medium. For instance, compared to the case of a dynamically supported system, the stellar ejecta may find it harder to find each other in a galaxy with net rotation, and eventually collide only at small angles and relative velocities. Furthermore, if we consider that the hot medium of a rotating galaxy may have inherited part of the angular momentum of the stars from which it originated,[4] then at a given orbital velocity the newly shed ejecta of a rotating galaxy may shock with the hot gas on average at a smaller velocity than in the case of the ejecta of a non-rotating galaxy, which would have imprinted no net rotation on its hot gas halo. According to these qualitative arguments we should expect that the kinetic energy of stellar ejecta is thermalized less efficiently in fast rotators. Ciotti & Pellegrini (1996) quantified this effect in the limit where none of the stellar rotational motion is thermalized, finding that the hot gas temperature could decrease by up to 30 per cent. Incidentally, in Fig. 8 this seems to be fairly close to the limit by how much colder the hot gas of fast rotators can get compared to the hot gas of slow rotators.

To conclude we note that in Fig. 8 the flat and X-ray underluminous slow rotator NGC 4365 displays a kT value in line with the behaviour of the other members of its class. This further indicates that if on one hand flattening could hamper the ability of a galaxy to retain its hot gas, on the other hand the degree of rotational support of a galaxy may also reduce the efficiency with which the kinetic energy inherited by the stellar ejecta is thermalized in the hot gas, which may be the case of fast rotators but not of a dynamically hot system such as NGC 4365.

3.3 Additional high X-ray resolution data

If the analysis presented in the previous two sections suggests a different specific hot gas content of fast and slow rotators, we need to keep in mind that these two kinds of early-type galaxies are rather relegated to low and high values for their dynamical mass $M_{\rm dyn}$, respectively (Paper III). In fact, this is in particular the case of the objects in the high X-ray resolution ATLAS^{3D} subsample that revealed also a possible role of $M_{\rm dyn}$ in driving the X-ray deficit of early-type galaxies (Fig. 7, right-hand panel), with the most massive fast rotators showing $L_{\rm X,\,gas}$ values that appear nearly as consistent with the input rate of kinetic energy from stellar mass loss as in the case of slow rotators (Fig. 6 and the right-hand panel of Fig. 8, where $M_{\rm dyn}$ is fairly traced by $L_K\sigma_e^2$). It would be therefore useful to observe the behaviour of other relatively massive fast rotators with $L_{\rm X,\,gas}$ estimates, as well as of slow rotators with lower $M_{\rm dyn}$ values than presently found in our high X-ray resolution sample, even if this will entail a loss of consistency in the X-ray or optical measurements.

For this reason, in Fig. 9 we added to the $L_K\sigma^2$–$L_{\rm X,\,gas}$ diagram also the other galaxies in the Boroson et al. sample, using their adopted central values for σ as well as their L_K and $L_{\rm X,\,gas}$ values, together with four more objects in the ATLAS^{3D} sample with $L_{\rm X,\,gas}$ measurements from other relatively large studies based on *Chandra* data, which have a few objects in common with the Boroson et al. that allow for some control on the consistency between $L_{\rm X,\,gas}$ estimates. These ATLAS^{3D} objects, for which we can rescale the $L_{\rm X,\,gas}$ values using our adopted distance estimates and have access to the rest of our ATLAS^{3D} imaging and integral field spectroscopic measurements, are the slow rotator NGC 6703 from the field sample of Mulchaey & Jeltema (2010) and the fast rotators NGC 4459, NGC 4494 and NGC 5845 from Athey (2007). Other $L_{\rm X,\,gas}$ compilations based on *Chandra* data, such as those of Diehl & Statler (2007) or Sun et al. (2007) either did not include other ATLAS^{3D} objects than those already considered by Boroson et al., or only featured ATLAS^{3D} objects that are deeply embedded in their ICM or group medium. Based on the deviations observed for the

[4] This is in fact quite possible given that the hot and warm phases are most likely in pressure equilibrium (as the inferred values for the ionized gas density suggest; see Mathews & Brighenti 2003, and references therein) and considering that fast rotators can display extended ionized gas discs that rotate in the same sense as the stars.

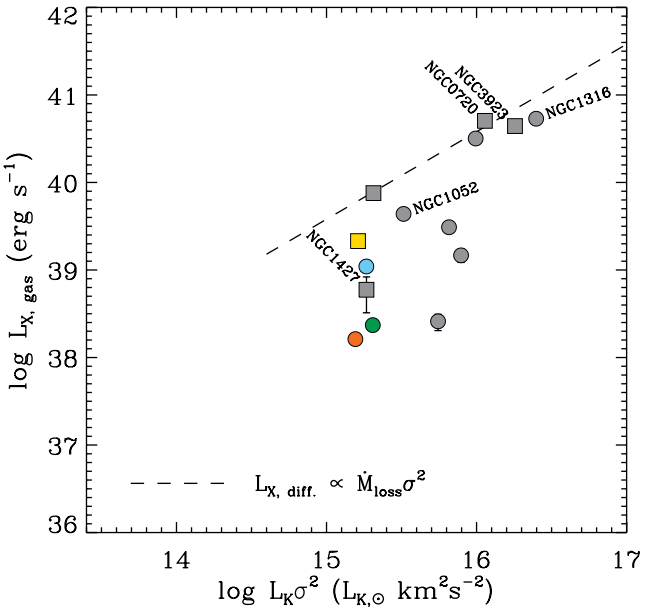

Figure 9. $L_K\sigma^2$ versus $L_{X,\,gas}$ diagram, similar to Fig. 6 and the right-hand panel of Fig. 8, but now showing either the remaining objects from Boroson et al. (2011, except M32) that are not in the ATLAS^{3D} sample (grey points) or galaxies with *Chandra* measurements of $L_{X,\,gas}$ and ATLAS^{3D} data (coloured points, from Athey 2007; Mulchaey & Jeltema 2010). The Boroson et al. objects are plotted using their values for $L_{X,\,gas}$, L_K and the central value for the stellar velocity dispersion σ, whereas for the additional ATLAS^{3D} galaxies we used our L_K and σ_e measurements and rescaled $L_{X,\,gas}$ using our adopted distance estimates. This also applies to NGC 720, for which SAURON data exist. Similarly to Fig. 8, square and round symbols indicate slow and fast rotators, respectively (see text for details on how such a separation was done for the Boroson et al. galaxies), with objects in the ATLAS^{3D} sample being colour coded according to our estimates for the average stellar age (from McDermid et al., in preparation). Finally, the labels indicate either objects with clear signs of recent star formation or particularly flat slow rotators (when inclined to the right and left, respectively). These additional data further suggest that the discrepancy in the hot gas content of fast and slow rotators may reduce or even disappear in very massive galaxies and that the presence of younger stellar subpopulations may increase the hot gas luminosity, while also revealing that galactic flattening may be a necessary but not sufficient reason for the $L_{X,\,gas}$ deficiency observed in a minority of slow rotators.

Boroson et al. objects that are in the ATLAS^{3D} sample (and have thus been observed with SAURON) we expect that for their remaining objects the $L_{X,\,gas}$ and $L_K\sigma^2$ measurements would be within 0.05 and 0.12 dex, respectively, of the values that they would have if they had been selected as an ATLAS^{3D} target, with no significant systematic deviations. Mulchaey & Jeltema have only two objects in common with the Boroson et al. sample, with $L_{X,\,gas}$ values that are consistent with theirs (assuming the same distance). Athey (2007) has 12 objects in common with Boroson et al., but in this case the reported $L_{X,\,gas}$ values are systematically lower by 0.18 dex, albeit with a similar scatter. Although these deviations are modest, for the sake of consistency, we did not consider objects that are not in the ATLAS^{3D} sample with $L_{X,\,gas}$ other than those of Boroson et al.

To assign the Boroson et al. galaxies that are not part of the ATLAS^{3D} sample to the slow- or fast-rotator families, we still adopted the $\lambda_{Re} = 0.31\sqrt{\epsilon_e}$ dividing line of Paper III but now resort to an indirect estimate for λ_{Re} and adopt the 2MASS K-band measurement of the minor- to major-axis ratio `k_ba` as a measure of the global flattening ϵ_e. To estimate λ_{Re} we use the relation between λ_{Re} and the $(V/\sigma)_e$ ratio given in Paper III (equation B1) and in turn derive the $(V/\sigma)_e$ ratio by applying the correction of Cappellari et al. (2007, their equation 23) to our best estimate of the (V_{max}/σ) ratio from long-slit data in the literature. The only exception to this procedure is represented by NGC 720, which is one of the 'special' objects observed in the course of the SAURON survey (de Zeeuw et al. 2002) and for which Cappellari et al. already reported values for σ_e, λ_{Re} and ϵ_e. Based solely on its λ_{Re} value, NGC 720 was considered a fast rotator by Emsellem et al. (2007), albeit already as an exceptional one by Cappellari et al., and falls now in the slow-rotator family when λ_{Re} is compared to $0.31\sqrt{\epsilon_e}$.

In Fig. 9 the objects with ATLAS^{3D} data (from Athey 2007; Mulchaey & Jeltema 2010) are colour coded as in Fig. 8 according to our global age estimates (from McDermid et al., in preparation) whereas for the remaining galaxies of the Boroson et al. sample we limited ourselves to identify only objects with clear signs of recent star formation episodes. These are NGC 1316, for which Silva, Kuntschner & Lyubenova (2008) used near-infrared data to establish a mean stellar age of ∼2 Gyr, and NGC 1052, for which Fernández-Ontiveros et al. (2011) report a global value for the NUV − r colour of 4.9, typical for early-type galaxies that experienced a recent star formation episode (e.g. Kaviraj et al. 2007). For the remaining sample galaxies of Boroson et al. it is difficult to draw a consistent picture of their stellar age, given the varying quality of the absorption-line strength measurements found in the literature (not always corrected for nebular emission) and the different choices for the models used to derive the stellar population properties.

The inclusion of these additional objects in our analysis confirms that fast rotators tend to have fainter X-ray haloes than slow rotators with similar $L_{X,\,diff}$ expectation values (from the thermalization of the kinetic energy brought by the stellar mass loss material), although Fig. 9 further indicates that such a discrepancy may reduce or even disappear as the dynamical mass of galaxies increases. As in the previous exceptional cases of NGC 4365 and NGC 5322, the slow rotator with the relatively faintest hot gas halo among the additional objects, NGC 1427, also happens to be a relatively flat galaxy (`k_ba` = 0.7; see D'Onofrio et al. 1995 for its long-slit kinematics). On the other hand, Fig. 9 introduces in our picture two flat and well-studied slow rotators, NGC 720 and NGC 3923 (with a `k_ba` value of 0.55 and 0.64, respectively; for the kinematics of NGC 3923 see Pellegrini et al. 1997), for which $L_{X,\,gas}$ appears well in line with the $L_{X,\,diff}$ prediction. Thus, it would appear that flattening can, but not necessarily does, drive a deficit in hot gas content of slow rotators. Finally, younger stellar populations are found in three out of the four fast rotators that in Fig. 10 sit the closest to the $L_{X,\,diff}$ prediction, consistent with a possible extra energy input from SNe in younger objects.

4 DISCUSSION

By combining photometric and integral field spectroscopic measurements with X-ray data of both low and high spatial resolution we have found that flat and rotationally supported early-type galaxies (i.e. fast rotators) tend to fall systematically short of the X-ray luminosity $L_{X,\,gas}$ that is expected if the hot gas radiation is sustained by the thermalization of the kinetic energy L_σ that the stellar mass loss material inherits from their parent stars. On the other hand, non- or slowly rotating galaxies (i.e. slow rotators), which are likely to be also intrinsically fairly round (Weijmans et al., in preparation), generally display $L_{X,\,gas}$ values in line with this model, and in fact also show hot gas temperatures that correspond well to the stellar

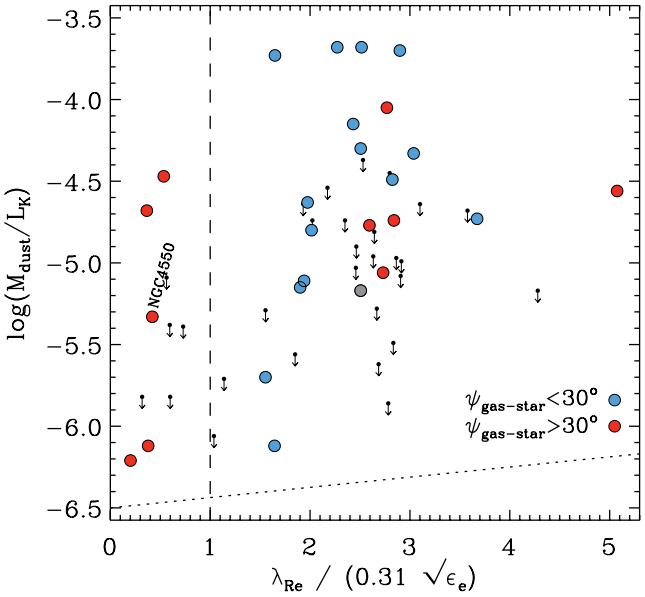

Figure 10. Specific dust mass content $\log(M_{\rm dust}/L_K)$ for the ATLAS^{3D} sample galaxies with *Herschel* data analysed by Smith et al. (2012) against their degree of rotational support, as quantified by the value of the $\lambda_{\rm Re}/(0.31\sqrt{\epsilon_{\rm e}})$ ratio that is also used to separate slow from fast rotators (vertical dashed line). The filled circles denote galaxies with $M_{\rm dust}$ detections, whereas the downward pointing arrows indicate objects with just $M_{\rm dust}$ upper limits. The dotted line shows the detection limit on the specific dust mass for this subsample, reflecting the fact that limits as low as $\log M_{\rm dust} = 5.0$ can be set across the whole considered range of $\lambda_{\rm Re}/(0.31\sqrt{\epsilon_{\rm e}})$ values whereas fast rotators extend to lower maximum $\log L_K$ luminosities than in the case of slow rotators. Except in one case (shown in grey), the objects with detected $M_{\rm dust}$ values also display diffused ionized gas emission, for which Davis et al. (2011) measured the angle between the angular momentum of the stars and the ionized gas. Objects with aligned ionized gas and stellar motions are shown in blue, whereas objects with a kinematic misalignment greater than 30° are shown in red. Such a kinematic information suggests that the ionized gas and dust of slow rotators is accreted, whereas most of the dustier fast rotators (i.e. with $M_{\rm dust}/L_K$ values in excess of what can be found in slow rotators) show aligned stellar and ionized gas motions, consistent with an internal origin of both the warm gas and dust. As $\lambda_{\rm Re}/(0.31\sqrt{\epsilon_{\rm e}})$ traces well the $L_{\rm X,\,gas}$ deficiency of fast rotators (Section 3.2), their ability to preserve more of their dusty stellar mass loss material could relate to the presence of a more tenuous hot gas medium compared to the case of slow rotators. In this respect, we note that the special slow rotator NGC 4550 (Emsellem et al. 2007) is very likely to be $L_{\rm X,\,gas}$ deficient given that it is intrinsically flat.

kinetic energy, as traced by the global stellar velocity dispersions within the optical regions of these galaxies $\sigma_{\rm e}$. This is not the case for fast rotators, which show nearly the same hot gas temperature across a range of $\sigma_{\rm e}$ values except for a few objects with younger stellar population that would appear to have hotter and also brighter gas haloes, possibly owing to the additional energy input from more recent SNe explosions. Such a discrepancy in the hot gas content of fast and slow rotators appears to reduce, or even disappear, for large values of the dynamical mass (beyond $\sim 3 \times 10^{11}\,{\rm M}_\odot$, corresponding in the ATLAS^{3D} sample to $\log L_K \sigma_{\rm e}^2 \sim 16$), whereas the few slow rotators with $L_{\rm X,\,gas}$ values considerably below the bar set by the thermalization of the kinetic energy brought by stellar mass loss material always appear to be relatively flat. This last result could suggest that it is the intrinsic shape of galaxies, rather than their degree of rotational support, that reduces their ability to retain the hot gas (Ciotti & Pellegrini 1996), although care is needed as there exist also flat slow rotators (albeit very massive) with $L_{\rm X,\,gas}$ perfectly in line with the $L_{\rm X,\,diff}$ expectation values.

The situation observed for slow rotators, whereby $L_{\rm X,\,gas} \sim L_\sigma$, is likely due to the fact that currently $L_{\rm SN} \sim L_{\rm grav}^-$ in these galaxies, so that most the Type Ia SNe energy is presumably used to steadily remove the stellar mass loss material and thus maintain a quasi-static hot gas atmosphere.[5] On the other hand, by virtue of their flattening and possibly also of their lower mass, $L_{\rm SN}$ exceeds $L_{\rm grav}^-$ in fast rotators so that these systems are actually degassing and thus display more tenuous and X-ray fainter hot gas haloes.

A systematic offset in the specific hot gas content of fast and slow rotators may be relevant to understand also the disparity between the incidence of molecular gas (Young et al. 2011) and associated episodes of recent star formation (Kuntschner et al. 2010) in these two classes of early-type galaxies (with slow rotators being devoid of both molecular gas and young stars), which in turn may link to an altogether different origin and fate for their gas (Sarzi et al. 2007). Indeed, much as the ICM or group medium may suppress the cold gas reservoir of galaxies falling in crowded galactic environments and drive the cosmic rise of lenticular galaxies (e.g. Dressler et al. 1997), the presence of a halo of hot gas around a galaxy may inhibit the star formation triggered either by the acquisition of gas-rich satellites or by the accumulation of stellar mass loss material. This is because small amounts of fresh gas would quickly heat up and evaporate in such an hot medium, by thermalizing its kinetic energy as it moves against the hot gas and inevitably shocks with it (e.g. Parriott & Bregman 2008, for stellar winds), and possibly also through thermal conduction (e.g. Nipoti & Binney 2007, for accreted gas). Furthermore, if hot gas haloes inherit part of the angular momentum of the galaxies that they enshroud (through the interaction between the hot gas and the stellar mass loss material, as advocated by Marinacci et al. 2011 in the case of disc galaxies), the accretion of gas from satellites could proceed differently depending on whether such material travels with or against the hot gas. In the latter case, for instance, ram-pressure stripping would be more efficient, since its strength depends on the square of the velocity relative to the hot medium.

Based on the distribution of the misalignment between the angular momentum of stars and ionized gas, Sarzi et al. (2006) already recognized (based on the smaller SAURON representative sample) a possible difference in the relative role of external gas accretion and stellar mass loss in fast and slow rotators, where in the latter class the warm gas would appear purely external in origin. Using the ATLAS^{3D} sample, Davis et al. (2011) not only confirmed this difference but also highlighted the impact of both a dense galactic environment (i.e. inside Virgo) and a large mass (for $M_K < -24$ or $\log L_K = 10.9$) in suppressing the acquisition of external gas by fast rotators. A bias towards finding corotating gas and stars in the most massive fast rotators is also consistent with the conclusion of Shapiro et al. (2010) that there exists two modes of star formation in fast rotators, such that in low-mass systems star formation is found throughout the galaxy and is triggered by minor mergers whereas in galaxies more massive that $\log M_{\rm dyn} \sim 10.95$ (which in the ATLAS^{3D} sample corresponds to $\log L_K \sim 10.8$) such an activity occurs only in central or circumnuclear regions and the

[5] In fact, as discussed in Pellegrini & Ciotti (1998) and Pellegrini (2012), even in such a quasi-static situation the gas flow is likely to be decoupled into an outflowing outskirts and a central inflow where radiative cooling outstrips the SNe energy feedback.

ionized gas rotates in the same sense as the stars. Interestingly, slow rotators would appear to accrete their ionized gas despite tending to be more massive and to reside in denser galactic environments than fast rotators (Davis et al. 2011). Perhaps, the present tendency of slow rotators to experience minor mergers can be regarded as a snapshot of their overall assembly history, since numerical simulations indicate that such a constant 'bombardment' is required in order to reduce the specific stellar angular momentum to the values observed in this class of objects (Bois et al. 2011; Khochfar et al. 2011, hereafter Paper VI and VIII, respectively).

In any event, the gas acquired in slow rotators does not appear to condense to a molecular phase and form new stars. Instead it must join the hot interstellar medium, most likely through thermal conduction as first suggested by Sparks, Macchetto & Golombek (1989) and later quantified by Nipoti & Binney (2007).[6] In fact, the lack of slow rotators with corotating gas and stars means that a similar fate also awaits any stellar mass loss material injected in such hot gas rich systems, whereas the systematic $L_{\rm X,\,gas}$ deficiency of fast rotators may allow for some fraction of this material to cool down amidst their more tenuous hot medium.

A good way of testing whether fast rotators, as opposed to slow rotators, can manage to cool down a fraction of their stellar mass loss material – thus possibly being more efficient at recycling such gas into new stars – would be to compare the specific content of the diffuse dust in these two classes of objects. Observed at infrared wavelengths, such diffuse dust can indeed trace more directly the material lost by stars than done for instance by the ionized gas component of the interstellar medium, in particular since the nebular flux may reflect also a varying ultraviolet ionizing flux from a number of different sources (Sarzi et al. 2010) whereas the dust of quiescent galaxies is mainly heated by the optical stellar radiation (e.g. Sauvage & Thuan 1992). Furthermore, the launch of the *Herschel Space Observatory* has now made it possible to probe the colder dust component of early-type galaxies and thus estimate more accurately their total dust mass $M_{\rm dust}$ than previously allowed by less sensitive instruments covering a more limited wavelength range, such as *IRAS*, *ISO* or *Spitzer* (see e.g. Goudfrooij & de Jong 1995; Athey et al. 2002; Ferrari et al. 2002; Temi, Brighenti & Mathews 2007).

Recently Smith et al. (2012) published $M_{\rm dust}$ estimates based on *Herschel* data for a sample of 62 nearby early-type galaxies, which include 57 objects from the ATLAS$^{\rm 3D}$ sample. Unfortunately, within this ATLAS$^{\rm 3D}$ subsample there are only five galaxies with both $M_{\rm dust}$ secure detections and $L_{\rm X,\,gas}$ measurements, making a direct comparison between the specific dust content and the X-ray properties in our sample galaxies not very meaningful. On the other hand, since the ATLAS$^{\rm 3D}$ objects with $M_{\rm dust}$ estimates have a range of $M_{\rm dyn}$ and $L_K\sigma_{\rm e}^2$ values that matches well that of the high X-ray resolution ATLAS$^{\rm 3D}$ subsample and of the additional objects that we have analysed in Sections 3.2 and 3.3, respectively, we can use our results to gauge the $L_{\rm X,\,gas}$ deficiency of the Smith et al. galaxies in our sample, and correlate that with their specific dust content.

For this reason, in Fig. 10 we show how the $\lambda_{\rm Re}/(0.31\sqrt{\epsilon_{\rm e}})$ ratio correlates with the specific dust content $M_{\rm dust}/L_K$ of the ATLAS$^{\rm 3D}$ objects analysed by Smith et al. This is similar to fig. 12 of that work, except that here we use L_K as a measure of the total stellar mass and regard $\lambda_{\rm Re}/(0.31\sqrt{\epsilon_{\rm e}})$ as an optical tracer of the $L_{\rm X,\,gas}$ deficiency compared to what is expected from the thermalization of the kinetic energy of the stellar mass loss material (Section 3.2). Furthermore, in Fig. 10 we also show objects with only upper limits on $M_{\rm dust}$ and colour code those with secure $M_{\rm dust}$ detections according to whether their ionized gas component shows an angular momentum that is considerably misaligned compared to that of the stars (i.e. by more than 30°).

Fig. 10 shows that fast rotators generally extend to larger values for the specific dust content than slow rotators, with very few fast rotators showing $M_{\rm dust}/L_K$ values reaching down to the values observed in the more dust-poor slow rotators. A similar message is conveyed also by the upper limits on $M_{\rm dust}/L_K$, in that they tend to constrain the specific dust content to consistently lower values as $\lambda_{\rm Re}/(0.31\sqrt{\epsilon_{\rm e}})$ decreases. In fact, all the slow rotators with secure $M_{\rm dust}$ detections in Fig. 10 show largely decoupled nebular and stellar motions consistent with an external origin for their gas, which suggests that the specific content of internally generated dust in these systems is probably much lower than currently inferred from their total far-infrared emission. On the other hand, most of the fast rotators with a specific dust content in excess of what is observed in slow rotators (i.e. for $M_{\rm dust}/L_K > -4.5$) display well-aligned gas and stellar angular momenta (in nine out of 10 cases, corresponding at most to a 20 per cent fraction of systems where the gas was accreted), suggesting that such a larger dust content originates from stellar mass loss material. This finding does not appear to be a result of sample selection. For instance, taken together all the fast rotators with $M_{\rm dust}$ detections are consistent with an even split between objects with internal and external origin for their gas just like for the entire ATLAS$^{\rm 3D}$ population of fast rotators (Davis et al. 2011). Furthermore, the fraction of objects in high-density environments (i.e. within the Virgo cluster) or with relatively large mass (i.e. $M_K < -24$) does not change when considering all the fast rotators with $M_{\rm dust}$ detections or just those with a higher specific dust mass content. This suggests that these otherwise important factors in determining the origin of the gas cannot entirely explain why the dustier fast rotators in Fig. 10 also happen to have corotating gas and stars.

Thus, once complemented with our kinematic information, the *Herschel* data of Smith et al. would appear to confirm that fast rotators have a larger specific dust content which relates to the fact that some fraction of the stellar mass loss material is allowed to cool in the less hostile hot gas medium of these objects, compared to the case of slow rotators. Such an ability of preserving some of their stellar mass loss material from joining the hot medium could also contribute (together with our previous conjecture on the possible role of a rotating X-ray halo) to the finding of Davis et al. (2011) that the most massive fast rotators do not seem to further acquire external gas, even when found in relatively sparse galactic environments. In fact, it may be even possible that in time such fast rotators build up a gaseous disc that is sufficiently massive to absorb counter-rotating gas from smaller satellites, which, on the other hand, would perturb more significantly the structure of less massive fast rotators. Yet, it is important to keep in mind here that not all fast rotators display dust or ionized gas, pretty much independent of galaxy mass and only mildly dependent on galactic environment (see table 2 of Davis et al. 2011). Even low-mass systems in the field, where both external accretion and internal recycling could occur, can be devoid of any gas. Apparently other mechanisms, beyond the scope of this paper, must operate to also remove gas from early-type galaxies.

A different specific hot gas content of slow and fast rotators and the likely different fate of their stellar mass loss material could also contribute to understand the fraction of rejuvenated early-type

[6] As a reference, Nipoti & Binney find that gas clouds of mass below 10^4–10^5 and 10^7–10^8 $M_\odot$ (at most, they are more likely to be 100 times smaller) would eventually evaporate as they fall in the hot medium of galaxies of baryonic mass of 3×10^{10} and 3×10^{11} $M_\odot$, respectively.

galaxies that has been estimated in much larger spectroscopic surveys of more distant galaxies. For instance, based on a consistent treatment of Sloan Digital Sky Survey spectra for over 3000 morphologically selected early-type galaxies, Thomas et al. (2010) revised the conclusion of Thomas et al. (2005, based on a more heterogeneous sample) and found that the impact of environment on the fraction of rejuvenated galaxies decreases with the mass of galaxies. In practice, for values of $M_{\rm dyn}$ above $\sim 10^{10.75}\,{\rm M}_{\odot}$ the fraction of galaxies with evidence of recent star formation steadily decreases till reaching values consistent with zero pretty much independent of galactic environment (see fig. 8 of Thomas et al. 2010). Given that our results are based on galaxies exceeding similar values of $M_{\rm dyn}$ (Fig. 7) we suggest that the internal processes regulating the star formation history at the massive end of the early-type galaxy population could be driven by the hot gas content of these objects and their ability to recycle the stellar mass loss material into new stars, which in turn could relates to the relative number of slow and fast rotators as well as the different degrees of $L_{\rm X,\,gas}$ deficiency displayed by the latter class of objects. For instance, where the fraction of rejuvenated objects in Thomas et al. starts to be negligible, around $M_{\rm dyn} \sim 10^{11.25}\,{\rm M}_{\odot}$, is incidentally also the point from which the fraction of slow rotators in the ATLAS$^{\rm 3D}$ sample shoots-up rapidly from values around 5–15 per cent to a fraction of $\sim$60 per cent for $M_{\rm dyn} \sim 10^{11.5}\,{\rm M}_{\odot}$ (fig. 11 of Paper III, but see also fig. 10 of Cappellari et al. 2013b, hereafter Paper XX), by which mass the hot gas content of fast rotators may not longer differ too much from that of slow rotators.

To conclude, we note that gravitational heating of infalling gas during minor mergers (in particular around the most massive galaxies; Dekel & Birnboim 2006; Khochfar & Ostriker 2008; Johansson, Naab & Ostriker 2009) is expected to deposit significant amount of energy in the hot gas. The relative contribution of this process compared to the thermalization of the kinetic energy inherited by the stellar mass loss material remains to be quantified, but unless to consider a very small efficiency for the latter mechanism, our results would suggest that – at least when considering the hot gas around galaxies that is not bounded by a group or cluster potential – gravitational heating presently does not play a dominant role. This would appear to contrast with the conclusions of Kormendy et al. (2009), although on this matter their analysis may pertain more to galaxies that are deeply embedded in their group or cluster potential and which we excluded from our work.

5 CONCLUSIONS

For a galaxy, being embedded in a corona of hot, X-ray-emitting gas can be a key element determining its recent star formation history. A halo of hot gas can indeed act as an effective shield against the acquisition of cold gas and can quickly absorb any stellar mass loss material, thus preventing its cooling and consequent recycling into new stars. In other words, the ability to sustain a hot gas halo can contribute to keep a galaxy in the so-called red sequence of quiescent objects.

Since the discovery by the *Einstein Observatory* of such X-ray haloes around early-type galaxies, the origin of the X-ray emission and the precise amount of hot gas around these galaxies have been the matter of long debates, in particular when trying to understand the rather loose correlation between the optical and X-ray luminosity of early-type galaxies. In the past, this situation resulted from the limited ability to isolate in earlier X-ray data the additional contribution from an active nucleus, the unresolved population of X-ray binaries and the X-ray emission from the ICM, although the use of heterogeneous optical data may have also contributed to such an impasse. Today, with new X-ray telescopes such as *Chandra* or *XMM* and large collections of both photometric and spectroscopic data it is possible to gain more insight on the hot gas content of early-type galaxies.

In this paper we have combined the homogeneously derived photometric and spectroscopic measurements for the early-type galaxies of the ATLAS$^{\rm 3D}$ integral field spectroscopic survey with measurement of their X-ray luminosity from X-ray data of both low and high spatial resolution, finding that the hot gas content of early-type galaxies can depend crucially on their dynamical structure. Specifically, in the framework of the revised kinematic classification for early-type galaxies advanced in the course of both the SAURON and ATLAS$^{\rm 3D}$ surveys (Emsellem et al. 2007, Paper III), we find that the following.

(i) Slow rotators have hot gas haloes with X-ray luminosity values $L_{\rm X,\,gas}$ that are generally consistent – across a fair range of $M_{\rm dyn}$ values – with what is expected if the hot gas radiation is sustained by the thermalization of the kinetic energy that the stellar mass loss material inherits from their parent stars, so that $L_{\rm X,\,gas}$ closely follows $L_K \sigma_{\rm e}^2$.

(ii) Fast rotators display $L_{\rm X,\,gas}$ values that tend to fall short of the prediction of such a model, and the more so the larger their degree of rotational support as quantified using the $\lambda_{\rm R}$ integral field parameter.

(iii) Such a $L_{\rm X,\,gas}$ deficiency in fast rotators would appear to reduce, or even disappear, for large values of the dynamical mass (beyond $\sim 3 \times 10^{11}\,{\rm M}_{\odot}$), whereas the few slow rotators with $L_{\rm X,\,gas}$ values considerably below the bar set by the thermalization of the kinetic energy brought by stellar mass loss material always appear to be relatively flat, nearly as much as on average fast rotators do.

(iv) Still consistent with a stellar origin for the heat needed to sustain their hot gas emission, slow rotators also display hot gas temperatures that correspond well to the global stellar kinetic energy, as traced by the stellar velocity dispersions measured within the optical regions $\sigma_{\rm e}$.

(v) Fast rotators, on the other hand, show similar values of T across a range of $\sigma_{\rm e}$, except for a few objects with younger stellar population that would appear to have both hotter and brighter X-ray haloes, possibly owing to the additional energy input from more recent SNe explosions.

These results indicate that the thermalization of the kinetic energy brought by stellar mass loss material, presumably through shocks and collisions of the ejecta with each other and the hot interstellar medium, sets a natural upper limit to X-ray emission originating from the hot gas bounded by the gravitational potential of present-day quiescent galaxies. This is observed mostly in the case of slow rotators, where the energy brought by Type Ia SNe is similar to that needed to steadily extract most of the mass lost by stars, thus helping maintain a quasi-static hot gas atmosphere. On the other hand, the fact that fast rotators as a class are most likely to be intrinsically flatter than slow rotators (with fast rotators being nearly as flat as spiral galaxies and slow rotators being much rounder and possibly triaxial; Weijmans et al., in preparation) leads us to interpret the $L_{\rm X,\,gas}$ deficit of fast rotators in light of the scenario of Ciotti & Pellegrini (1996) whereby flatter galaxies have a harder time in retaining their hot gas. Flattening indeed reduces the binding energy of the gas, which would cause SNe to drive global outflows in fast rotators, thus reducing their hot gas density and X-ray luminosity. The finding that the few $L_{\rm X,\,gas}$-deficient slow rotators also happen to be relatively flat would lend further support to this hypothesis,

although care is needed as there are also flat slow rotators with $L_{X,\,gas}$ perfectly in line with what is observed in the more standard and round slow rotators. We also note that if the intrinsic shape of a galaxy could determine the ability of a galaxy to retain its hot gas halo, the degree of rotational support could further lower the efficiency with which the kinetic energy carried by the stellar mass loss material is thermalized in the hot gas. Indeed, this efficiency appears to reach its peak in the dynamically supported slow rotators, where T traces well σ_e.

Finally, using recent *Herschel* measurements for the diffuse dust emission of early-type galaxies and the kinematic information on the relative motions of stars and gas provided by our integral field spectroscopic observations, we have also shown that fast rotators have a larger specific dust content compared to slow rotators, and that this is likely due to the fact that some fraction of the stellar mass loss material is allowed to cool down in the more tenuous medium of these objects. Such an ability to recycle the stellar mass loss links well with the fact that among massive early-type galaxies, only fast rotators have detected molecular gas and display signs of recent star formation, something that cannot occur in slow rotators where both stellar mass loss and accreted material quickly fizzles in the hot medium.

ACKNOWLEDGEMENTS

We wish to thank the anonymous referee whose comments helped much in improving the paper. MS is indebted to Gary Mamon, Silvia Pellegrini, Nicola Brassington, Martin Hardcastle and Luca Cortese for useful discussion, and to both ESO and the Institut d'Astrophysique de Paris for their hospitality during much of the preparation of this paper. MS acknowledges support from an STFC Advanced Fellowship ST/F009186/1. MC acknowledges support from a Royal Society University Research Fellowship. This work was supported by the rolling grants 'Astrophysics at Oxford' PP/E001114/1 and ST/H002456/1 and visitors grants PPA/V/S/2002/00553, PP/E001564/1 and ST/H504862/1 from the UK Research Councils. RLD acknowledges travel and computer grants from Christ Church, Oxford and support from the Royal Society in the form of a Wolfson Merit Award 502011.K502/jd. SK acknowledges support from the Royal Society Joint Projects Grant JP0869822. RMM is supported by the Gemini Observatory which is operated by the Association of Universities for Research in Astronomy, Inc., on behalf of the international Gemini partnership of Argentina, Australia, Brazil, Canada, Chile, UK and USA. TN and MBois acknowledge support from the DFG Cluster of Excellence 'Origin and Structure of the Universe'. NS and TAD acknowledge support from an STFC studentship. The authors acknowledge financial support from ESO. We acknowledge use of the NASA/IPAC Extragalactic Database (NED) which is operated by the Jet Propulsion Laboratory, California Institute of Technology, under contract with the National Aeronautics and Space Administration.

REFERENCES

Athey A. E., 2007, PhD thesis, University of Michigan, Michigan (arXiv:0711.0395)
Athey A., Bregman J., Temi P., Sauvage M., 2002, ApJ, 571, 272
Bender R., Surma P., Doebereiner S., Moellenhoff C., Madejsky R., 1989, A&A, 217, 35
Bois M. et al., 2011, MNRAS, 416, 1654 (Paper VI)
Boroson B., Kim D.-W., Fabbiano G., 2011, ApJ, 729, 12
Brighenti F., Mathews W. G., 1996, ApJ, 470, 747
Canizares C. R., Fabbiano G., Trinchieri G., 1987, ApJ, 312, 503
Cappellari M., 2008, MNRAS, 390, 71
Cappellari M. et al., 2006, MNRAS, 366, 1126
Cappellari M. et al., 2007, MNRAS, 379, 418
Cappellari M. et al., 2011a, MNRAS, 413, 813 (Paper I)
Cappellari M. et al., 2011b, MNRAS, 416, 1680 (Paper VII)
Cappellari M. et al., 2012, Nat, 484, 485
Cappellari M. et al., 2013a, MNRAS, 432, 1709 (Paper XV)
Cappellari M. et al., 2013b, MNRAS, 432, 1862 (Paper XX)
Ciotti L., Ostriker J. P., 2001, ApJ, 551, 131
Ciotti L., Pellegrini S., 1996, MNRAS, 279, 240
Ciotti L., D'Ercole A., Pellegrini S., Renzini A., 1991, ApJ, 376, 380
Davies R. L. et al., 2001, ApJ, 548, L33
Davis T. A. et al., 2011, MNRAS, 417, 882
Dekel A., Birnboim Y., 2006, MNRAS, 368, 2
D'Ercole A., Ciotti L., 1998, ApJ, 494, 535
de Zeeuw P. T. et al., 2002, MNRAS, 329, 513
Diehl S., Statler T. S., 2007, ApJ, 668, 150
D'Onofrio M., Zaggia S. R., Longo G., Caon N., Capaccioli M., 1995, A&A, 296, 319
Dressler A. et al., 1997, ApJ, 490, 577
Ellis S. C., O'Sullivan E., 2006, MNRAS, 367, 627
Emsellem E. et al., 2007, MNRAS, 379, 401
Emsellem E. et al., 2011, MNRAS, 414, 888 (Paper III)
Eskridge P. B., Fabbiano G., Kim D.-W., 1995a, ApJS, 97, 141
Eskridge P. B., Fabbiano G., Kim D.-W., 1995b, ApJ, 442, 523
Faber S. M., Gallagher J. S., 1976, ApJ, 204, 365
Faber S. M., Jackson R. E., 1976, ApJ, 204, 668
Fernández-Ontiveros J. A., López-Sanjuan C., Montes M., Prieto M. A., Acosta-Pulido J. A., 2011, MNRAS, 411, L21
Ferrari F., Pastoriza M. G., Macchetto F. D., Bonatto C., Panagia N., Sparks W. B., 2002, A&A, 389, 355
Forman W., Schwarz J., Jones C., Liller W., Fabian A. C., 1979, ApJ, 234, L27
Forman W., Jones C., Tucker W., 1985, ApJ, 293, 102
Goudfrooij P., de Jong T., 1995, A&A, 298, 784
Johansson P. H., Naab T., Ostriker J. P., 2009, ApJ, 697, L38
Kaviraj S. et al., 2007, ApJS, 173, 619
Khochfar S., Ostriker J. P., 2008, ApJ, 680, 54
Khochfar S. et al., 2011, MNRAS, 417, 845 (Paper VIII)
Kim D.-W., Fabbiano G., 2004, ApJ, 611, 846
Kormendy J., Fisher D. B., Cornell M. E., Bender R., 2009, ApJS, 182, 216
Krajnović D. et al., 2011, MNRAS, 414, 2923 (Paper II)
Kundu A., Whitmore B. C., 2001a, AJ, 121, 2950
Kundu A., Whitmore B. C., 2001b, AJ, 122, 1251
Kuntschner H. et al., 2010, MNRAS, 408, 97
Liu J., 2011, ApJS, 192, 10
Marinacci F., Fraternali F., Nipoti C., Binney J., Ciotti L., Londrillo P., 2011, MNRAS, 415, 1534
Mathews W. G., Brighenti F., 2003, ARA&A, 41, 191
Mathews W. G., Loewenstein M., 1986, ApJ, 306, L7
Matsushita K., 2001, ApJ, 547, 693
Mulchaey J. S., Jeltema T. E., 2010, ApJ, 715, L1
Mulchaey J. S., Davis D. S., Mushotzky R. F., Burstein D., 2003, ApJS, 145, 39
Nipoti C., Binney J., 2007, MNRAS, 382, 1481
O'Sullivan E., Forbes D. A., Ponman T. J., 2001, MNRAS, 328, 461
Parriott J. R., Bregman J. N., 2008, ApJ, 681, 1215
Pellegrini S., 2011, ApJ, 738, 57
Pellegrini S., 2012, in Kim D. W., Pellegrini S., eds, Astrophysics and Space Science Library, Vol. 378, Hot Interstellar Matter in Elliptical Galaxies. Springer, New York, p. 21
Pellegrini S., Ciotti L., 1998, A&A, 333, 433
Pellegrini S., Held E. V., Ciotti L., 1997, MNRAS, 288, 1
Pipino A., Kawata D., Gibson B. K., Matteucci F., 2005, A&A, 434, 553
Santos W. A., Mendes de Oliveira C., Sodré L., Jr, 2007, AJ, 134, 1551
Sarazin C. L., Irwin J. A., Bregman J. N., 2000, ApJ, 544, L101

Sarzi M. et al., 2006, MNRAS, 366, 1151
Sarzi M. et al., 2007, New Astron. Rev., 51, 18
Sarzi M. et al., 2010, MNRAS, 402, 2187
Sauvage M., Thuan Th. X., 1992, ApJ, 396, 69
Shapiro K. L. et al., 2010, MNRAS, 402, 2140
Silva D. R., Kuntschner H., Lyubenova M., 2008, ApJ, 674, 194
Skrutskie M. F. et al., 2006, AJ, 131, 1163
Smith M. W. L. et al., 2012, ApJ, 748, 123
Sparks W. B., Macchetto F., Golombek D., 1989, ApJ, 345, 153
Statler T. S., Emsellem E., Peletier R. F., Bacon R., 2004, MNRAS, 353, 1
Sun M., Jones C., Forman W., Vikhlinin A., Donahue M., Voit M., 2007, ApJ, 657, 197
Temi P., Brighenti F., Mathews W. G., 2007, ApJ, 660, 1215
Thomas D., Maraston C., Bender R., Mendes de Oliveira C., 2005, ApJ, 621, 673
Thomas D., Maraston C., Schawinski K., Sarzi M., Silk J., 2010, MNRAS, 404, 1775
Trinchieri G., Fabbiano G., 1985, ApJ, 296, 447
van den Bosch R. C. E., van de Ven G., Verolme E. K., Cappellari M., de Zeeuw P. T., 2008, MNRAS, 385, 647
White R. E., III, Sarazin C. L., 1991, ApJ, 367, 476
White R. E., III, Sarazin C. L., Kulkarni S. R., 2002, ApJ, 571, L23
Young L. M. et al., 2011, MNRAS, 414, 940
Zhang Z., Gilfanov M., Bogdan A., 2012, A&A, 546, A36

This paper has been typeset from a TEX/LATEX file prepared by the author.